

Advanced Virgo Conceptual Design

VIR-042A-07

The Virgo Collaboration

edited by

The Advanced Virgo Team*

October 26, 2007

* Contact person: G.Losurdo - e-mail: losurdo@fi.infn.it

Contents

1	Introduction	1
2	Advanced Virgo design	2
2.1	Baseline configuration	2
2.2	Main open options	2
2.3	Reference design parameters	3
2.4	A possible timeline	3
3	Sensitivity	5
4	Laser	11
4.1	Preliminary requirements	11
4.2	Baseline design	11
4.3	Possible fiber design	12
4.3.1	Status of the related R&D	13
5	Injection system	14
5.1	General requirements	14
5.2	Schematics	14
5.3	EOM and RF Modulation	16
5.4	Faraday isolator	16
5.5	Larger clear aperture Faraday isolator	19
5.6	Power control and stabilization	19
5.7	IMC	20
5.8	Resonant suspended IMC for AdV	20
5.8.1	Scattered light in the IMC	21
5.8.2	Jitter suppression	21
5.8.3	IMC instabilities	22
5.8.4	IMC suspension strategy	22
5.8.5	Resonant IMC: summary	22
5.9	Fiber IMC option for AdV	23
5.9.1	Status of the related R&D	23
5.10	Mode Matching Telescope	24
5.10.1	Non-degenerate recycling cavity	24
5.10.2	Adaptive system	24
5.11	Layout(s)	25
5.12	Status of the related R&D	25
6	Mirrors	27
6.1	Substrates	28
6.2	Polishing	28
6.3	Coating	29
6.4	Metrology	30
6.5	Cleaning	30

6.6	Charge buildup	31
6.6.1	Mirror Charge Control	31
6.6.2	Status of R&D	33
7	Thermal compensation	34
7.1	TCS design	34
7.1.1	Compensation plate	34
7.1.2	Test mass shielded ring heaters	35
7.1.3	TCS sensors	36
7.1.4	Beam splitter compensation	36
7.1.5	Higher order modes	36
7.1.6	A possible scheme	37
7.1.7	Status of the related R&D	37
8	Detection system	38
8.1	DC detection and needed modifications	38
8.1.1	Power noise considerations	39
8.1.2	Requirements	39
8.1.3	Status of the related R&D	41
9	Optical design	42
9.1	Signal recycling	42
9.1.1	Quantum correlations	42
9.1.2	Other connected changes and side effects	43
9.2	Degeneracy of recycling cavities	43
9.3	Wedges and pick-off beams	45
9.4	Beam size and geometry	47
9.4.1	The TEM ₀₀ mode	47
9.4.2	Higher Order Laguerre Modes	49
10	Interferometer sensing and control	54
10.1	Length sensing and control	54
10.1.1	Status of the related R&D (CALVA)	55
10.2	Alignment sensing and control	56
11	Superattenuators	61
11.1	IP modifications and tilt control	61
11.1.1	Status of the related R&D	62
11.2	Tiltmeters	62
11.2.1	Status of the related R&D	64
11.3	SR SA	64
11.4	Short SA upgrade	64
11.5	Suspensions Last Stage: marionette reference mass	65
11.5.1	Status of the related R&D	66
11.6	Suspensions Last Stage: New marionette	66

11.7	Suspensions Last Stage: new reference mass	67
11.8	Suspensions Last Stage: electrostatic actuators option	68
11.8.1	Status of the Related R&D	69
12	Monolithic suspensions	74
12.1	Geometry and dimensions	74
12.1.1	Mirror geometry	74
12.1.2	Bouncing mode	75
12.1.3	Violin modes	75
12.1.4	Fiber shape	75
12.2	The ribbon option	76
12.3	Ears machining	78
12.3.1	Status of the related R&D	78
12.4	Mirror local control system	78
12.4.1	Status of the R&D	78
13	Electronics, controls and data acquisition	81
14	Vacuum system modifications	83
14.1	Requirements	83
14.2	New link tubes	83
14.2.1	Baffles	84
14.2.2	Brewster links	84
14.3	SR tower	84
14.4	UHV chamber improvements for AdV	85
15	Infrastructure modifications for environmental noise reduction	86
	References	87

1 Introduction

The effort of the Virgo Collaboration towards the design of a 2nd generation detector started in 2005 with the *Advanced Virgo White Paper* [1], The White Paper has shortly defined the list of expected changes of the Virgo setup to upgrade it to Advanced Virgo (AdV). Afterwards, four working groups have been set up to deepen the design effort:

- **WG1:** optical configuration;
- **WG2:** laser and input optics;
- **WG3:** vibration isolation, suspensions and mirrors;
- **WG4:** electronics.

This document is the main outcome of the WGs activity. Its aim is to propose a conceptual design of the detector. Since the R&D program for AdV is far to be complete some important options are still open. The document propose a baseline for AdV, together with the possible alternative or auxiliary options for some of the subsystems.

The main goals of AdV are:

- to improve the Virgo sensitivity by a factor ~ 10 in the whole frequency range;
- to be in data taking at the same time as Advanced LIGO [2] (2014).

These two objectives have been kept into account for the definition of the baseline.

2 Advanced Virgo design

2.1 Baseline configuration

In this section we list the technical choices that are considered as AdV *baseline*. In making such a selection we have taken into account:

- the technical readiness of the chosen systems;
- when not yet ready, the importance of the system in order to reach a competitive sensitivity or to simplify the detector design, together with the probability to be ready in time.

The AdV baseline (see fig.1) is defined as follows:

- **Interferometer configuration:** dual-recycled interferometer;
- **Laser:** Solid state laser developed at LZH (sec. 4);
- **IMC:** 144 m suspended resonant IMC (sec. 5);
- **Mirrors:** 42 kg (35cm in diameter, 20 cm thick), state of art coatings (sec. 6);
- **Thermal compensation:** combination of CO₂ laser and heating rings (sec. 7);
- **Detection:** in-vacuum photodiodes, DC detection (sec. 8);
- **Beam geometry:** Gaussian beam, waist in the center of the Fabry-Perot cavities, larger spot on the cavity mirrors (sec. 9);
- **Vibration isolation:** SA with new IP legs, tilt control, Marionette Reference Mass, new reference mass compliant with the thicker mirror, coil-magnet actuators (sec. 11);
- **Suspensions:** cylindrical fused silica fibers (sec. 12).

2.2 Main open options

Beside the chosen configuration, a few options remain open. They might replace the corresponding baseline choice and be integrated in the AdV final design in case the R&D outcomes are positive:

- fiber laser (sec. 4.3);
- fiber IMC (sec. 5.9);
- non-Gaussian beam (higher order Laguerre modes) (sec. 9.4);
- 60 kg mirrors (sec. 6);
- alternative suspension geometries: dumbbell fibers or ribbons (sec. 12.2);
- electrostatic actuators (sec. 11.8).

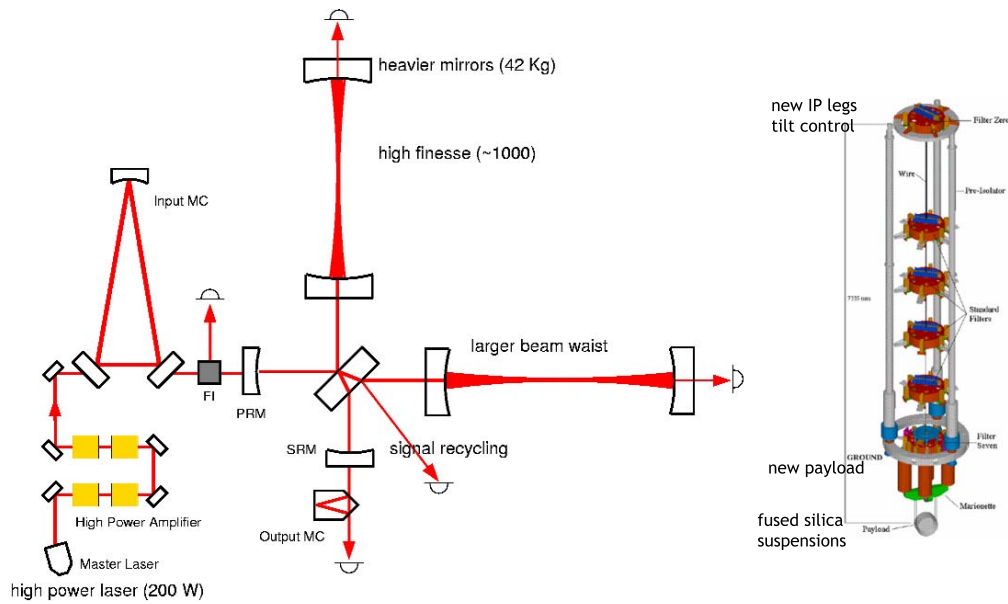


Figure 1: The AdV baseline design.

All the listed options (except the choice of the suspensions geometry) have an important impact on the design of some parts of the detectors. Therefore a final choice has to be made at the end of 2008, when the first AdV Design Review will be held.

2.3 Reference design parameters

Some important design parameters for AdV are summarized in table 1 and compared with the corresponding ones in Virgo. Most of them are to be confirmed since the configuration and tuning of the detector will be decided in the next months after a thorough system study. Namely, parameters such as the power on the BS, the transmittance of the mirrors, the cavity finesse, will be the outcome of further studies of the Optical Simulation and Design group and have to be defined in the next months¹.

2.4 A possible timeline

The work of installation, integration and validation of the subsystems is expected to last about two years. This period should include also the precommissioning of some detector parts such as the superattenuators and the input mode cleaner.

We propose to proceed with a two steps strategy:

¹ For instance, the sensitivity curve presented afterwards have been calculated assuming that the laser spot on the cavity mirror has a radius of 60 mm. This is the same value used in the Advanced LIGO simulation but the feasibility of this choice has to be verified.

Subsystem	Virgo	ADV Virgo
Laser Power	20 W	200 W
Input ITF power	7 W	125 W (TBC)
Power on BS	~300 W	~2.9 kW (TBC)
Input mirror transm.	0.12	0.007 (TBC)
End mirror transm.	40 ppm	5 ppm (TBC)
Arm cavity finesse	50	885 (TBD)
SR mirror transm.	none	0.04 (TBD)
Mirror mass	21 kg	42 kg
Mirror diameter	35 cm	35 cm

Table 1: The main parameters of the baseline AdV.

- **power-recycled AdV:** the SR mirror is not installed in this phase. The interferometer is commissioned with high power. This would allow to practice with the effects high power/high finesse in a simpler configuration. A possible sensitivity curve in this configuration is shown in fig. 3.
- **dual-recycled AdV:** installation of the SR mirror and commissioning of the full detector. A possible sensitivity curve in the dual-recycled case is shown in fig. 3, 4.

If the installation starts in 2011, the commissioning of the power recycled AdV can start at the beginning of 2013. One to one and half year of commissioning, mostly dedicated to learning how to cope with an high power and high finesse interferometer, should be foreseen to reach a good sensitivity in the power recycled configuration. A first AdV science run could be then possible in 2014. After the run a second upgrade must be scheduled, with the installation of the SR mirror. This break could be exploited to further upgrade the detector (e.g. by replacing the laser/IMC with the fiber solution if it is technically ready and if it is useful). The commissioning of the dual recycled interferometer (see fig. 3) will encounter new problems, especially on the locking side. Nevertheless, at this stage, the experience done with high finesse cavities and a thorough locking simulation effort started in the previous years are expected to be helpful.

This is not the only possible two step strategy. Another possibility is to start immediately with the dual-recycled AdV but keeping the power low and increase it progressively once the interferometer control has been learned.

3 Sensitivity

The sensitivity curves shown in this section have been plotted using the MATLAB *BENCH* code developed at LIGO [3] and adapted to AdV. The curves shown are based on some assumptions:

- **optical readout noise:** it is hereafter also defined *quantum noise*² and is calculated using the Buonanno-Chen model [4]. It assumes the DC detection scheme. In the models used so far the cavity finesse is 885, the power recycling factor is 23.5 and the power on the BS is about 2.9 kW. These are just *possible* choices [5], to be further evaluated;
- **coating thermal noise:** a coating dissipation $\phi_{\text{TaO}_2} = 2.4 \cdot 10^{-4}$ for the tantala is assumed [6], corresponding to a coating dissipation $\phi_{\text{coat}} \approx 1.6 \cdot 10^{-4}$. The beam radius on the cavity mirrors is assumed to be 6 cm;
- **mirror brownian noise:** the brownian noise of the fused silica mirrors is less important than the coating thermal noise. However, it must be remarked that if coil-magnet actuators will be used magnets will be glued on the mirror. The corresponding increase of dissipation and the effects on the sensitivity must be calculated;
- **suspension thermal noise:** cylindrical fibers with a radius of 206 μm are considered (750 MPa stress);
- **newtonian noise:** the Cella-Cuoco model is used [7]. It must be remarked that such model predicts a noise level higher than the one expected at LIGO.

On the basis of the choices mentioned above, we have calculated the AdV sensitivities without (fig. 2) and with (fig. 3) signal recycling. Once the SR mirror transmittance (0.04 in the case of fig. 3) has been chosen a further tuning is possible by changing its working position in a sub-micron range (see fig. 4). A comparison with the Virgo sensitivity is shown in fig. 5.

Inspirial range (Mpc)	BNS	BBH
Virgo (design)	13	58
Virgo+ (with mon. susp.)	49	250
Advanced LIGO	175	975
AdV (no SR, fig.2)	97	265
AdV (with SR, fig.3)	121	856

Table 2: The averaged inspirial range for BNS and BBH for the AdV configurations corresponding to fig. 2 and 3, compared with the similar Virgo, Virgo+ and Advanced LIGO figures.

In table 2 the BNS and BBH inspirial ranges obtained for the sensitivities of fig. 2 and 3 are compared with the ones of Virgo, Virgo+ and Advanced LIGO.

² In this model the shot noise and radiation pressure noise are considered as intimately related and treated as one.

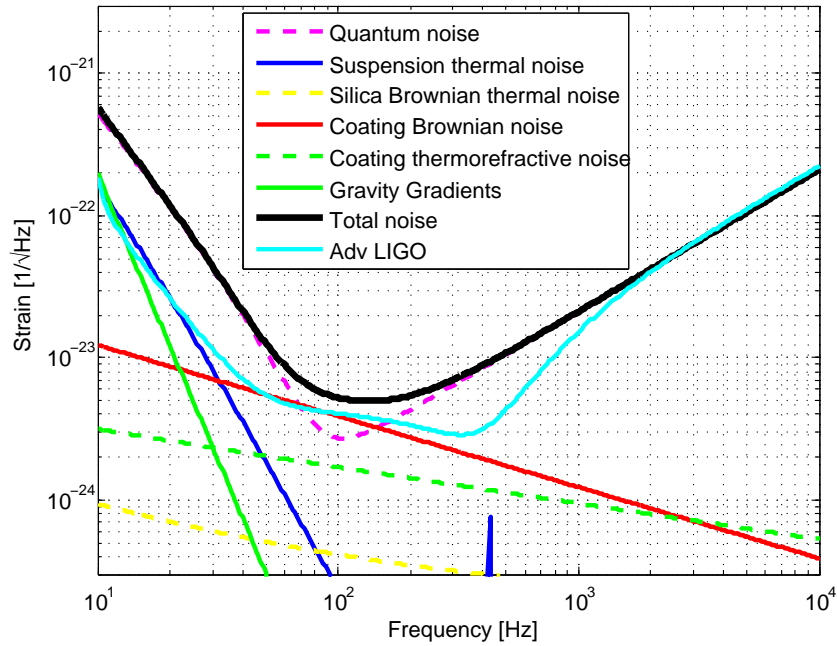


Figure 2: Possible sensitivity of the power-recycled AdV (no SR mirror). It has been calculated with 125 W of laser power entering the interferometer, cavity finesse of 885, PR factor of 23.5.

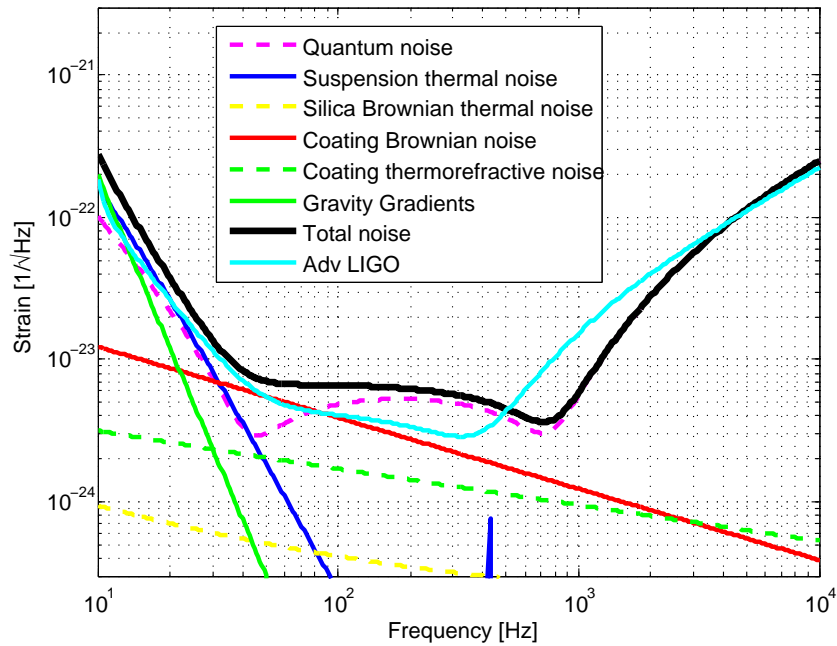


Figure 3: Possible sensitivity of the dual-recycled AdV. It has been calculated with SR mirror transmittance of 0.04, 125 W of laser power entering the interferometer, cavity finesse of 885, PR factor of 23.5.

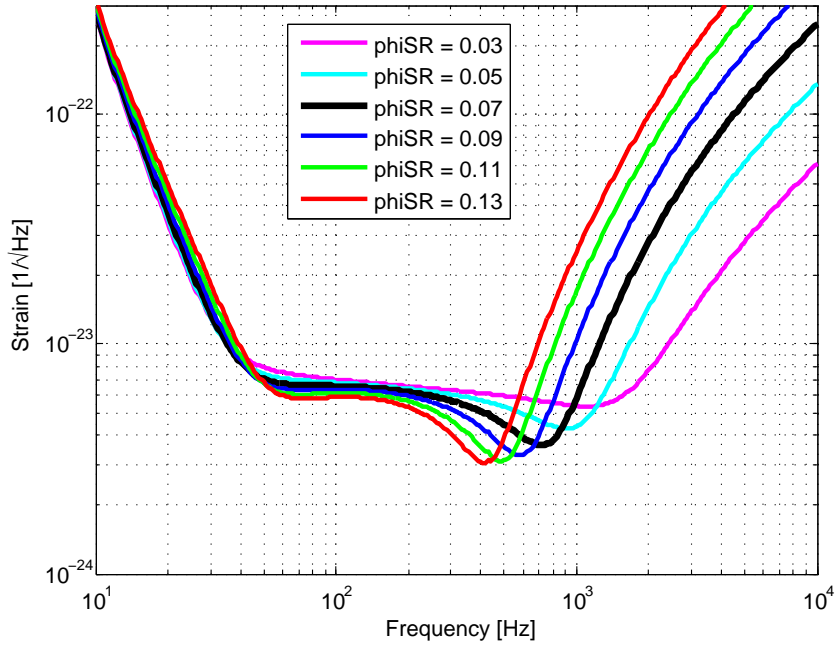


Figure 4: Tuning the AdV sensitivity by changing ϕ_{SR} . The black curve ($\phi_{SR} = 0.07$) corresponds to the reference sensitivity of fig. 3.

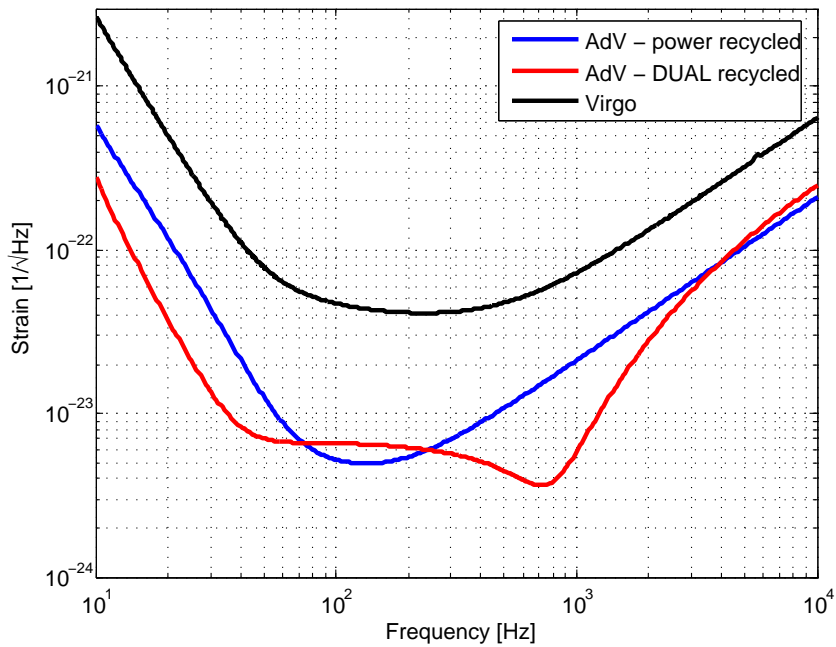


Figure 5: The virgo design sensitivity is compared with the AdV one for the two cases of fig. 2 and 3.

Advanced Virgo Conceptual Design:

PART 1:

Interferometer

4 Laser

The AdV laser will deliver 200 W. It will be stabilized in frequency and amplitude and should respect a set of requirements concerning beam geometry and beam jitter. The set of requirements has not yet been finalized. The data given below are preliminary. They result from our experience of Virgo, extrapolated to the expected performance of AdV. Some data are taken from the documents of Advanced LIGO, since the design and performances of both detectors will be comparable. The definition of the final requirements will require more calculations and modeling studies, taking into account the design changes. For instance, the following numbers assume the same filtering of the input mode cleaner (IMC) as for Virgo and the same prestabilization scheme (ie a laser prestabilized on the IMC and a power stabilization performed after the IMC). They also assume that the contrast and asymmetries of the interferometer, and the precision of alignment and longitudinal controls, will remain the same as they are in Virgo, and that the OMC (output mode cleaner) is unchanged. The possible change to the DC detection might relax some constraints in RF range compared to Virgo while needing some relevant effort in the low frequency range.

4.1 Preliminary requirements

Requirement	Value
Power	200 W
Frequency noise	$PSD(f) < 10/f \text{ Hz}/\sqrt{\text{Hz}}$ above 10 Hz
Power noise	$RIN(f) < -180 \text{ dB}/\sqrt{\text{Hz}}$ (for $10 \text{ Hz} < f < 10 \text{ kHz}$)
Beam jitter	$< 10^{-6} \text{ rad}/\sqrt{\text{Hz}}$
Beam geometry	$M^2 < 1.05$ (h.o.m. content $< 5\%$)

Notice that³:

- the frequency noise figure refers to the prestabilized laser at the input of IMC;
- In case we select a DC detection scheme, the laser power noise at RF frequency will not be significant. If we keep using RF detection, the requirement will be $RIN(f_{\text{mod}}) < -170 \text{ dB}/\sqrt{\text{Hz}}$ (shot noise for 1W detected power);
- the specification on laser beam geometry might require a pre-mode cleaner.

4.2 Baseline design

The laser baseline design (see fig. 6) consists in a 1-2W master laser (Nd-YAG at 1064 nm) similar to the present Virgo master laser, amplified to 200W by Nd-YVO₄ diode pumped

³ These numbers are very preliminary and have to be refined. The 200W laser assumes a 65% overall transmission for the injection optics

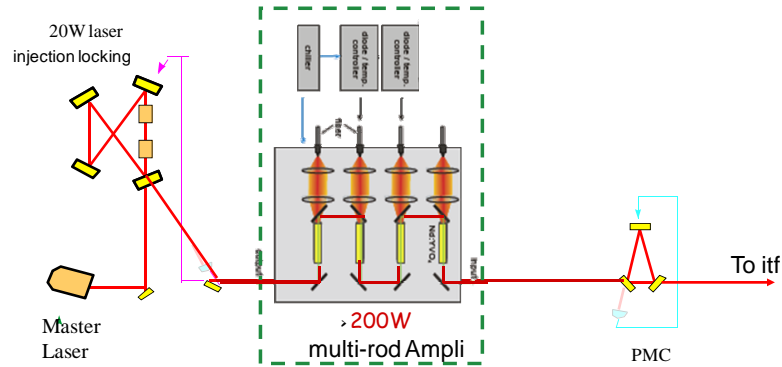


Figure 6: Laser system baseline design: a master laser of 2W injection-locks a first stage of 20W laser which is amplified through a multi-rod amplifier, to deliver 200W output power. A pre-mode cleaner might be useful to clean out the residual high order modes.

amplifiers. Another possible straightforward solution would be to keep the Virgo+ laser system up to 50W, and to complete it by the high power amplifier that Laser Zentrum Hannover has already developed for Advanced LIGO. With that choice, we are already sure to reach the right power level and to fulfill approximately the requirements:

- the frequency noise should not be very different from the noise of the Virgo laser, and the frequency control scheme and control electronics could be kept, with only slight upgrades;
- the beam geometry may not be excellent, but a low finesse pre-mode-cleaner can solve the problem.

4.3 Possible fiber design

We are also considering the possibility to move towards a fibre technology:

- fibre amplifiers, using large mode area (LMA) fibres and photonic crystals have demonstrated the capability to generate very high power single mode beams (up to kW level, limited by the pump diodes), and, because of many potential applications, the domain of high power fibred systems is developing rapidly;
- the fibre core is made of silica, doped with Ytterbium (Yb). This system absorbs light around 976 nm, and provides amplification in the range 1040-1070 nm. The conversion efficiency is very high in terms of photon number, and in terms of energy per photon. The optical efficiency of a fibre amplifier exceeds 70%, and the technology of the pumping diodes at 976 nm is good with lifetimes over 100000 hours.
- different schemes are possible, from an all fibred system starting with a fibre oscil-

lator, followed by fibre modulators (power, frequency/phase, polarization) for the lasers controls and by high power amplifiers, all welded together, to a Virgo-like low power system followed by the high power fibre amplifier. In all cases the beam would be directly delivered to the injection bench at the end of a fibre. This would suppress the need for alignment systems and should make the injection system much more immune to vibrations and acoustics.

- but we still have to check that the nonlinearities of the fibre (Brillouin effect, mainly) will not create too much additional fluctuations nor too much spurious light, that mode-mixing in the fibre will remain low enough, that the polarization of the light can be maintained. High power fibre amplifiers have not yet been tested at the required low noise levels and an R&D effort is necessary.

In conclusion, the baseline solution is safe. The fibre solution is much more promising if higher power is requested in the future, and it offers new possibilities: in particular, it is possible to generate, to amplify, and to transport in a fibre a single high-order mode LP_{0n}. This should improve the sensitivity of the interferometer in the low frequency range around 100 Hz, where the thermal noise of the mirrors will dominate, because it uses the mirrors surface much more homogeneously than the usual Gaussian mode (TEM₀₀). For the same reason, it will reduce the thermal distortions of the mirror.

Very likely, the initial laser system for AdV will be the baseline solution, progressively replaced by fibre elements during short interruptions of the operation: replacing the last stage of amplification should be the first step. A complete strategy has to be elaborated, once we will know more precisely what is possible to do.

4.3.1 Status of the related R&D

A research grant has been obtained from Agence National de la Recherche in order to build a 200 W fibre amplifier. EGO is providing a research grant which will provide the salary for a PhD student to work on that subject. The study is just starting now.

5 Injection system

5.1 General requirements

The Input Optics subsystem of AdV takes care of the optics downstream of the high power laser, and of the interface of these optics and the laser itself. The whole system must deliver a beam with the required power, geometrical shape, power, frequency and angular stability. Given the 200 W power delivered by the High Power AdV laser, it is required:

Requirement	Value
Transmission to the ITF	$> 50\%$
Non-TEM ₀₀ power	$< 5\%$
Intensity noise	$2 \times 10^{-9} / \sqrt{\text{Hz}}$ at 10 Hz
Beam Jitter	$< 10^{-9}$ rad/ $\sqrt{\text{Hz}}$ ($f > 100$ Hz)

An EOM system will provide the needed RF phase modulation (for control and sensing purposes). A matching and steering system in air will be used either to couple the beam into the in-vacuum suspended input mode cleaner (IMC) or into the fiber IMC. The IMC will geometrically clean the beam and reduce its amplitude and lateral fluctuation. The resonant IMC will also serve as first stage of frequency pre-stabilization. After the IMC an intensity stabilization section will provide the signal for stabilizing the laser RIN of the beam. An in-vacuum Faraday isolator will prevent interaction of the ITF (interferometer) reflected light with the IMC and laser system. Finally, an ITF mode matching telescope will give to the beam the correct dimension for matching with the interferometer. This telescope can be different, if a marginally stable recycling cavity or a stable recycling cavity are used. A thermal adjustment of the mode matching can be part of the system.

5.2 Schematics

The schematic layout will include an in-air (outside vacuum) part and an in-vacuum part, namely:

- In-air
 - EOM for RF modulation
 - Faraday isolation
 - Collimation and steering optics
- In-vacuum
 - Input Mode Cleaner
 - Faraday isolation

- Matching telescope
- Steering optics
- Power stabilization

At present, there is more than one option still considered as possible for the final configuration of the IO layout: one option is the at present Reference Solution (see Fig.7: this solution is close to the one adopted by Advanced LIGO, and can benefit of the already several years R&D activity carried out by LIGO in this area for speed up the implementation.

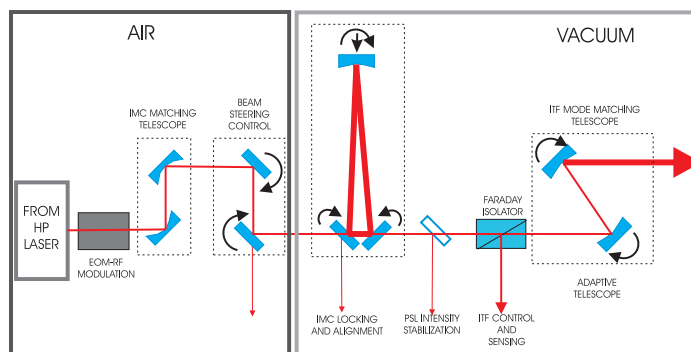


Figure 7: Schematic of the AdV Reference IO solution: the laser will be either a SSL (solid state laser) or a fiber laser. The IMC (input mode cleaner) will be a suspended resonant triangular cavity. The telescope will include an adaptive system, either thermal (mirror heating) or with an adaptive steering mirror.

The other solution (Fibre Solution, see Fig. 8) is considering the possibility to replace the input mode cleaner with a fiber component.

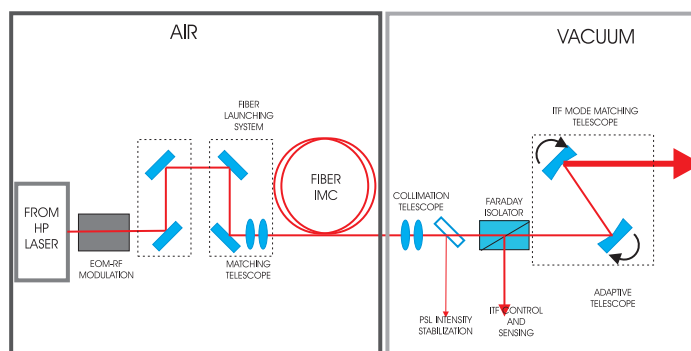


Figure 8: Schematic diagram of the AdV IO solution in which the suspended IMC is replaced by a fiber IMC

An innovative R&D activity, which has no counterpart in LIGO, is going on about this subject, and in the next years a decision about the feasibility of this solution has to be taken. A possible path would plan starting with the Reference Solution and later provide the possibility to shift to the Fibre Solution. This solution will include also an alternative system for the frequency pre-stabilization.

- Reference Solution (with solid state laser (SSL) source):
 - High power optical components
 - Suspended resonant input mode cleaner (IMC)
 - Suspended bench(es) supporting Faraday isolator and matching telescope
- Fibre Solution:
 - High power optical components
 - Fibre IMC
 - Suspended bench(es) supporting Faraday isolator and matching telescope

5.3 EOM and RF Modulation

RF or DC detection are still open options for AdV. RF modulation will be anyhow used for the control of the interferometer, both for longitudinal locking and alignment. The main difference between the EOM to be used in AdV and Virgo resides in that the power that the first EOM will have to withstand will be 10 times higher (200 W instead of present 20 W). Thermal effects will become more significant ([8]), and the choice of RTP (or RbTiOPO₄, rubidium titanyl phosphate), a less absorbing material than presently used KTP, would be recommended ([9]). Also wedged cut RTP (and AR coated) crystals would represent an improvement ([10]). Requirements in AdV for EO modulation will also be different, in particular depending on whether RF or DC detection will be used: many of these parameters will affect the driving electronics and signal generator choice. Indicative numbers for the single sideband noise requirements (modulation phase noise) can be found in [11], and for modulation index noise (amplitude noise) in [12]. More than one modulation frequency will likely be used in AdV, either for control and for monitoring. The increased sensitivity and complexity of the interferometer will make important addressing the problems of sidebands on sidebands generation. The solution of this problem could imply novel EOM topology (see for example [13]), which have still to be fully tested and assessed.

5.4 Faraday isolator

Light back reflected by the ITF towards the IMC has already been an issue in Virgo. This problem will be more significant with the higher power of AdV. The solution for this problem has been the use of an in-vacuum Faraday isolator placed between the IMC and

the ITF. Either in the case in which a suspended IMC or a fiber IMC will be used, an in-vacuum Faraday isolator between the interferometer and the IMC will be necessary. With the higher AdV laser power (200 W input power), standard Faraday isolator will exhibit loss of optical isolation, owing to thermally induced birefringence, and very high thermal lensing. In order to attain a good level of optical isolation (≈ 40 dB) a specifically designed Faraday isolator has to be used, including depolarization compensation and a passive correction of its thermal lensing. A design developed in many years of extensive experimentation has already been adopted by LIGO, and should fit also to AdV needs.

The main questions to be addressed, as far as the in vacuum Faraday isolator is concerned, could be summarized as:

- withstand high average power (300 W) on long periods;
- provide enough optical isolation;
- compensate depolarization and thermal lensing;
- provide good transmission and reflection;
- not to introduce beam steering;
- not to be too big and heavy.

At present there is no precise requirement about how much optical isolation is to be obtained by the in-vacuum optical isolator. There is a general agreement that, in presently operating interferometer, an isolation of about 30 dB is satisfactory. There is neither any test nor any reliable simulation setting limits for the needed optical isolation. Virgo experience shows that a lack of optical isolation (less than 20 dB) makes the locking acquisition of the recycling cavity difficult or impossible, and some visible effects on the low frequency ITF alignment start to be visible. The present setup makes it not possible to modify remotely the isolation, in order to perform tests on effects on sensitivity. No experience in this direction is available either in LIGO. It is generally agreed that in the next interferometers an isolation better than 40 dB should be provided, even in view of the fact that experienced degradation of the isolation with the change of power and when going from air to vacuum have been observed. The prototype for high power operation in LIGO, which will be used already in Enhanced LIGO, exhibits an optimal optical isolation exceeding 49 dB at more than 100 W input laser power. However, simulations of thermo-optical effects in TGG show that the isolation ratio changes when going from air to vacuum, depending on the laser power going through the Faraday crystal. These simulations have been confirmed both in Virgo experience and in LIGO bench tests. In order to optimize the optical isolation, a remote tuning will be necessary (analogous to that planned for Virgo+).

Optical isolation performances, according to LIGO experience (which has been carried on in collaboration with Novgorod IAP group), strongly depends, at laser power level typically exceeding 50 W, on thermal depolarization effects in TGG crystal. Depolarization

ha to be ascribed mainly to the temperature dependence of the Verdet constant and to photoelastic effect [14]. Many years of extensive experience in the Novgorod group [15] have lead to an optical design of a Faraday isolator which compensate thermal depolarization effects. The optical isolation provided by the prototypes reaches 49 dB with more than 100 W laser input power.

The schematics of the candidate Faraday isolator for AdV is described in detail in [15]: it comprises an input polarizer, a $\Lambda/2$ waveplate, two TGG crystals rotating the polarization by 22.5, separated by a -67.5 polarization rotating Quartz Rotator, and an end polarizer. A difference, with respect to LIGO, could be the use of a larger free aperture TGG crystal: the LIGO isolator has a free aperture of 20 mm. In AdV, if the beam coming out from the IMC will have a diameter of 1 cm, a 25-30 mm aperture Faraday isolator should be more convenient, in order to avoid beam size reduction.

The candidate polarizers are Calcite Wedged polarizers (about 4.3 wedge) or Brewster Thin Film polarizers.

Further improvements to the Faraday isolator will be the possibility to remotely compensate a loss of optical isolation in vacuum and a compensation of the thermal lensing. In Virgo it has already been experienced a drop of optical isolation of the Faraday isolator when going from air to vacuum: after tuning the isolator for optimal isolation in air, a loss of about 10 dB of isolation has been measured. This results have been confirmed by the experience in LIGO performed with the prototype isolator (see also [16]). In order to correct this effect, already in Virgo+ a system is planned, which entails the insertion of a $\Lambda/2$ waveplate, mounted on a motorized mount, between one polarizer and the TGG crystal. By remotely rotating the waveplate by less than one degree it should be possible to correct this effect. Thermal lensing in the in-vacuum Faraday isolator has also already been experienced in Virgo. The induced thermal lensing results in a mismatching of the beam with respect of the ITF. The thermally induced focal length in Virgo, with 10 W input power in the Faraday isolator (almost 20 W considering the reflection of the unlocked ITF) was of the order of 100 m. In this case, the induced mismatching is of the order of 1%, thus not affecting the ITF performances. Scaling the present Virgo situation to the AdV higher power (200 W), the computed resulting induced focal length is of about 13 m, thus yielding an unacceptable mismatch of 37%. Passive compensation will use DKDP (deuterated potassium dihydrogen phosphate, KD_2PO_4) calibrated bar mounted after the Faraday isolator. The thickness of the bar is critical for exact lensing compensation, the exact dimensions depending on DKPD and TGG parameters. These parameters are not exactly known a priori, this making it difficult to cut exactly the slice with the right length. The effect of the DKDP slice could be changed by changing the crystal temperature: a remote temperature modification should be implemented. The DKDP should be contacted to a heater/cooler (e.g. a Peltier placed below the thermally conductive mount of the DKDP), thus allowing to tune the lens compensation.

The dimensions of the Novgorod-IAP Faraday isolator are quite big: $60.5\text{cm} \times 12.7\text{cm} \times 26.5\text{cm}$. The weight is about 14 kg. The clear aperture is 20 mm. In order to accommodate the beam coming out of the IMC (5 mm waist at present) a larger clear aperture would be desirable (25-30 mm). The rotator crystals are TGG, polarizers still to be de-

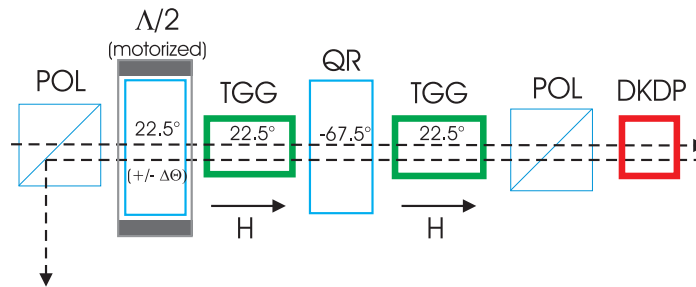


Figure 9: High Power in-vacuum Faraday isolator

cided (Calcite or Brewster thin film). All materials have to be vacuum compatible. The accommodation of this large device in the input bench vacuum vessel of Virgo could be an issue. A solution for the available space has to be found.

5.5 Larger clear aperture Faraday isolator

A possibility to use a larger clear aperture Faraday isolator has been considered: at the state of the art, it would be possible to have efficient Faraday isolators with a clear aperture up to 25-30 mm: this apertures would accommodate a 5 mm semidiameter beam without any clipping problem. The development of a larger aperture Faraday would require some R&D, since it has never been made up to now, and would probably lead to larger dimensions and weight (however, likely less than 700 mm and 20 kg). This possibility has to be kept open, since it would allow to use the beam of the 144 m IMC (5 mm semidiameter) without reducing its size with a telescope: a reducing telescope could introduce astigmatism and produce parasitic reflections. Moreover, reducing the size of the IMC beam, means that the mode matching telescope should have a larger magnification power (need of a faster mode matching telescope). Therefore, the possibility of having a larger Faraday isolator would yield several significant advantages. The problem would be mainly in its dimensions.

5.6 Power control and stabilization

Power amplitude fluctuation can generate noise in the ITF both through a fringe offset and differential radiation pressure, owing to cavity reflectivity asymmetries. At the AdV power (> 100 W input power) the differential radiation pressure is expected to dominate. Functional requirements, computed in the assumption of 1% asymmetry and 50 ± 1 beam splitter reflectivity, give limits on the amplitude fluctuations at the level of $10^{-9}/\sqrt{\text{Hz}}$ at 10 Hz.

The power stabilization loop will be an extension of the system used by present Virgo. The signal for the power stabilization is picked up in vacuum after the IMC and fed back to the laser source. A further stabilization stage could use as error signal the power in the power recycling cavity.

5.7 IMC

The laser light must be frequency and spatially stabilized before it can be used in the interferometer. The input mode cleaner (IMC) provides active frequency stabilization through feedback to the laser, passive frequency noise suppression above its cavity pole frequency, and passive spatial stabilization at all frequencies. The input mode cleaner also reduces higher order modal content of the laser light, suppressing beam jitter. For the AdV IMC, we have selected 2 possible configurations that are presented in this document. The first one is the traditional triangular mode cleaner which is currently used in all the interferometric gravitational waves detectors. The reference solution for AdV is with a 144 m triangular resonant suspended IMC.

The second solution should consist in an optical fiber that should spatially filter the laser beam before entering the interferometer (see sec. 5.9).

5.8 Resonant suspended IMC for AdV

The present Virgo IMC is a Fabry-Perot triangular cavity with a high finesse (about 1,000). The triangular configuration is preferred with respect to others since it generates almost no back reflection to the laser, thus providing an improved isolation. The cavity configuration is flat-flat-curved. Two flat suspended mirrors define the base and act as the input and output couplers. The third mirror (curved one) is suspended in the Mode-Cleaner tower 143.5 meter far from the injection tower.

Two solutions have been considered for a suspended IMC for AdV: the first one consists in keeping the same Virgo IMC length, using the current infrastructures. The second consists in reducing the IMC length to reduce scattered light problems we are currently struggling against in Virgo.

The advantages of a shorter IMC would be:

owing to the larger incidence angle at the end MC mirror, there will be less scattered light in the beam path inside the cavity;

the beam size of the beam exiting the IMC would be smaller.

The first point would reduce the coupling of the light reflected back by the ITF with the light going to the the ITF. The second point would allow the use of a smaller Faraday isolator (20 mm clear aperture would be sufficient with a 3 mm semidiameter beam).

The main problem which arises, if we want to use a shorter IMC, involves infrastructure modifications, because in this case we need to build and install a new tower that will be

at least 20 meters far from the current injection tower. This is a huge and expensive work since the present building may be too small to accommodate a vacuum tank. It seems not conceivable for AdV.

The advantage of keeping the current infrastructures resides in its low cost and easy implementation. However, a lot of work has to be performed in order to reduce the light scattered inside the IMC (see sec. 5.8.1). In particular, we have to work on coating and surface roughness specifications together with LMA lab and the substrate provider. As mentioned above (5.5, the beam waist at the output of the IMC being about 5 mm with the 144-m-long IMC, the possibility to use a larger clear aperture FI (at least 25 mm) should be kept open, otherwise a telescope that will reduce the beam size in order to avoid clipping in the FI has to be used (like in present Virgo). It should be noted that, both in the case of a shorter IMC, and in the case of an IMC beam reduced in size to go through a 20 mm Faraday, the mode matching telescope should have the same magnification power: requirements on the mode matching telescopes would be less stringent only in the case in which the 5 mm semidiameter IMC beam were used (i.e. with a larger clear aperture Faraday isolator).

5.8.1 Scattered light in the IMC

The incoming light impinging on the mode cleaner end mirror is scattered by the mirror surface, which is not perfect. Thus, due to the small angle of the mode cleaner (about $3 \cdot 10^{-4}$ rad), a part of the scattered light can propagate in the opposite direction and be sent back to the laser. The biggest problem is that the two traveling waves can interfere and create some fringes at the level of the IMC alignment photodiodes. These interferences can spoil the performances of the IMC control and add some noise to the laser beam sent in the ITF [17]. A solution to reduce the scattering from the IMC end mirror is to decrease the IMC length but as it has already been discussed in the previous section this configuration seems too expensive. Another possibility consists in improving the surface quality of the IMC end mirror in order to reduce back-scattered light coming from this mirror. It seems reasonable that with this kind of mirror and a 40 dB isolation FI we can get rid of the fringes visible in the IMC alignment signals.

5.8.2 Jitter suppression

Beam pointing noise specifications for AdV are 10^{-9} rad/ $\sqrt{\text{Hz}}$ after the input mode cleaner [18], considering that the input mode-cleaner controls are enough stable to not reintroduce beam jitter noise due to suspended Mode-cleaner motion. Because higher-order modes are suppressed by the input mode cleaner, beam jitter is also decreased. The filtering efficiency depends on two things: the finesse F has to be as high as possible and the IMC has to be non-degenerate (higher-order modes should not be resonant in the IMC). The main concern about beam jitter is IMC control. We have to deeply study this point in order to not reintroduce jitter noise due to IMC motion.

Most often the beam pointing noise is dominated by acoustic and thermal effects induced noise on components in free-space propagation (EOM, FI, etc. . .). The R&D program that aims to study thermal effects in those components will probably help a lot improving beam pointing noise.

5.8.3 IMC instabilities

- **Radiation pressure and IMC motion:** The IMC and ITF mirrors will be subjected to incremental radiation pressure changes as the input power is changed. Since the IMC mirror is lighter than the ITF mirrors and the power stored in the IMC cavity is more than two times the power stored in the long arms, it is likely that radiation pressure could be visible with the IMC end mirror. Nevertheless, it has been shown [19] that it should be possible to lock the IMC with an incident power of 180 watts increasing the IMC end mirror mass to 900 g. Further studies are needed to define how heavy should be the IMC end mirror in order to minimize the radiation pressure phenomenon.
- **IMC thermal effects:** Substrate and coating absorption of the IMC mirrors will lead to change in the radius of curvature of the three IMC mirrors [20]. Evaluation of the output beam characteristics has to be given in order to foresee a compensation of this thermal effect is necessary.
- **IMC frequency noise:** The frequency stability of the laser beam at the output of the IMC is known to be strongly dependent on the IMC length. The frequency stabilization loop has to be reviewed in order to minimize this noise and to reach the specifications on frequency noise that are required by the interferometer.

5.8.4 IMC suspension strategy

In case we choose a triangular IMC, we have to define how the 3 mirrors have to be suspended. We have 2 possibilities:

- The IMC end mirror has its own suspension and the 2 flat mirrors are fixed on a dihedron which is put on a suspended bench (Virgo current configuration).
- The 3 mirrors are suspended individually, this solution can be interesting to remove the dihedron resonances that are visible in the dark fringe for Virgo.

This item has to be deeply investigated to determine the strategy to choose.

5.8.5 Resonant IMC: summary

For the AdV resonant IMC, two possible configurations have been discussed

- The one using the current infrastructure: 144-m-long IMC.

- A shorter IMC, to reduce scattered light coming from the IMC end mirror. This solution would require a new building to host the IMC end mirror.

The second configuration seems not feasible for AdV since it requires a huge infrastructural work and a non-negligible extra-cost for AdV project. The resonant IMC seems to be compliant with the requirements of AdV but thermal effects, radiation pressure and scattering, in particular, have to be deeply studied before considering this configuration as valid. The reference layout for this configuration would be:

- 144-m-long triangular resonant IMC
- Reducing size telescope (from 5 mm to about 3 mm waist beam)
- 20 mm clear aperture Faraday isolation
- Mode Matching Telescope: magnification from 3 mm in the Faraday isolator to about 1 cm in the center of the AdV cavity arms

The possibility to use a larger clear aperture Faraday isolator would make not necessary to use the reducing size telescope and would impose less requirements on the mode matching telescope (R&D activity).

Moreover IMC control scheme and the suspension itself of the new suspended mode-cleaner have to be upgraded to fulfill the requirements in term of frequency and beam jitter noise foreseen for AdV.

5.9 Fiber IMC option for AdV

As already suggested above, a fibre optic can be used to clean the output beam of the laser or even to convert this beam to a desired high order mode. The main advantages over a resonant mode cleaner would be the absence of maintenance, the simplification of the controls (all alignment controls suppressed except the positioning of the fibre end), and the simplification of the optical scheme. No more frequency pulling by the mode cleaner motion, no more need to adjust precisely the modulation frequency, etc ... The only drawback would be the need for more active control of the frequency and power fluctuations, since we would lose the filtering effect of the long IMC above 500 Hz.

5.9.1 Status of the related R&D

This study started two years ago, with the initial goal to replace the mode-cleaner by a singlemode fibre, using the new technology of hollow photonic crystal fibres (PCF). The potential advantages, which have been confirmed, are a higher transmission and the absence of frequency selectivity, which permits the transmission of sidebands (or even of auxiliary laser beams). This R&D today is the continuation of the previous work, where the hollow PCF will be replaced by a solid silica LMA (large mode area) Bragg fibre. This mainly requires the manufacturing of an adequate LMA single-mode fibre, preferably with a polarization maintaining structure. The new fibre, to be delivered soon, will be

tested for coupling efficiency, beam geometry, phase, power, and polarization noises, at different power levels, depending on the highest power available at the time of the test.

5.10 Mode Matching Telescope

The design of the mode matching telescope (MMT) for AdV will be close to the Virgo one: it will be an off-axis parabolic telescope, consisting in 2 parabolic mirrors longitudinally separated by around 700 mm. Current telescope is confocal because the manufacturers claimed they couldn't provide parabolic mirrors with the needed characteristics to build an afocal telescope. This may not be true anymore. An afocal telescope design should relax in a significant way the tuning tolerances and the requirements for the mirrors. Both options are under study. The MMT should deliver the light from the Faraday Isolator to the ITF with the proper mode content. The coupling efficiency of light into the main interferometer shall be 0.95 or greater in TEM_{00} . Actually, it should be about 0.99 as already demonstrated with the current parabolic MMT. The major issue is actually to meet the constraints imposed by the diameter of the optical free aperture at the output of the telescope (300 mm) and the physical dimensions of the Suspended Input Bench. A detailed design and a study to recover any error within the range of the mirrors' specifications by repositioning the 2 parabolic mirrors are under progress.

5.10.1 Non-degenerate recycling cavity

The MMT will be different in case a non-degenerate recycling cavity will be decided. The design specifications for a non-degenerate recycling cavity have not been finalized yet, and they should be decided in alignment with the requirements for the MMT. Design study activity is still required on this item. However, it is expected that the requirements on the MMT will become less stringent in case of a non-degenerate recycling cavity.

5.10.2 Adaptive system

The difficulty in obtaining a good matching has already been evident in Virgo. With higher circulating power, spurious higher modes will become a more serious issue. In order to optimize the matching, an adaptive matching system will be provided. A reference solution for this problem is a thermal heating, using an ancillary laser, of one mirror of the mode matching telescope. An alternative solution, still being investigated, would be the use of an adaptive mirror as one of the in vacuum steering mirrors ([21], [22]). In this case, issues connected to adaptive mirror actuator noise (normally piezoelectric) should be taken into account and investigated.

5.11 Layout(s)

A simplified layout of the AdV Injection Bench is shown in Fig.10. In order to accommodate the IMC input mirrors, the mode matching telescope and the Faraday isolator in the small space available in the injection tower, part of the layout has to be mounted below the bench (the Faraday isolator). The Reference Cavity, which is mounted below the Suspended Input Bench in Virgo, has to be moved outside the tower.

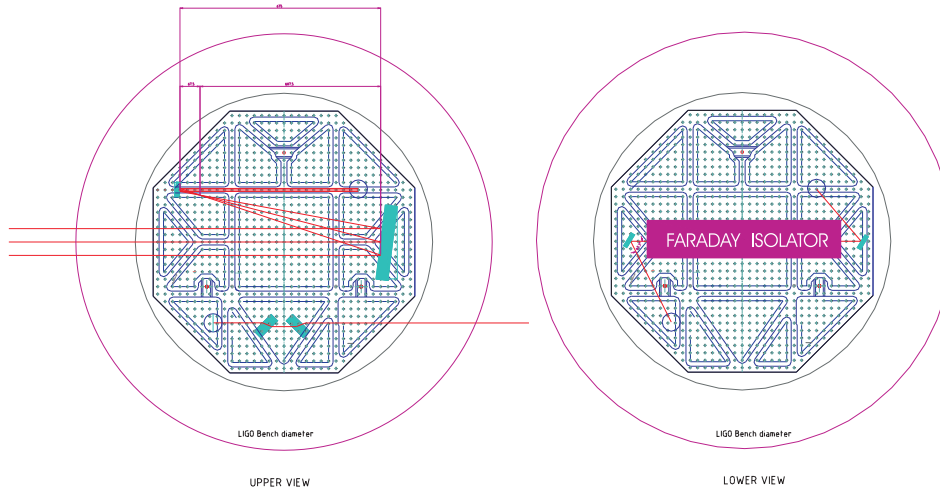


Figure 10: Schematic diagram of the AdV IO solution in which the suspended IMC is replaced by a fiber IMC

5.12 Status of the related R&D

Input Optics for AdV can benefit of the many years of R&D already performed by LIGO. LIGO has already dedicated many years and resources in investigating high power components like electro-optical modulators and Faraday isolator. The results obtained by LIGO are available. In consideration of the state of advancement of the R&D of LIGO, Virgo has opted for relying as much as possible on LIGO research, and concentrate his effort mainly on alternative solutions, like the fiber IMC. Hence, the AdV reference solution, will be largely based on the results obtained in LIGO.

On the other hand, starting from the results of LIGO, further investigations in collaboration with LIGO are being performed also in Virgo. One R&D program has been started on fiber IMC (see sec. 5.9). Another three years R&D program is about high power optical components for AdV has already started, with the purpose to define some important elements for AdV. This R&D is meant to cover both the present reference solution and be open for the fiber IMC solution. In this program a high power (200 W) commercial laser is used, and is starting testing components analogous to those designed for Advanced LIGO, mainly as far as the thermal effects are concerned (thermal lens, birefringence,

misalignments): in LIGO the tests on input optics components have not been performed with input power larger than 100 W, so the measurements to be performed in Virgo will give additional information. The purpose is on one side to tune the components for the purposes of AdV, to test alternative solutions and to develop expertise in Virgo. In the R&D program the high power laser and respective instrumentation has been purchased, and investigations are going on concerning the passive thermal compensation of the Faraday isolator: this experience is not available in LIGO yet. The further step will be the test, in air and in vacuum, of a full Faraday isolator, with the hope to be able to get a larger aperture rotator. A program for testing specifically designed (by Lyon-LMA laboratories) Brewster polarizers is also planned: this should give more information concerning the possibility to use these polarizers instead of calcite wedged polarizers. In the next year the study of EOM in different configuration is planned. The purpose of this R&D program is to finally provide the components to be used in the reference solution for AdV, in particular: an in-vacuum Faraday isolator, an EOM system, a passive thermal compensation of the Faraday thermal lensing, an adaptive correction of the mode matching telescope using an adaptive mirror.

Depending on the results of the R&D on the fiber IMC, the investigation could be diverted in next year towards fiber systems, if the fiber solution will become the reference solution for AdV.

6 Mirrors

As it is shown in fig. 3, mirrors play a crucial role in the sensitivity of AdV. On one side the mechanical losses in the coating determine the quality factor of the mirror and as a consequence the displacement of the mirror surface due to its thermal vibration. On the other side the optical losses in the coatings determine the amount of power which is lost in the Fabry-Perot cavity and as a consequence the power that is stored in the recycling cavity. This quantity determines the quantum noise which is expected to limit the sensitivity at the higher frequencies. R&D is ongoing at LMA to improve the mechanical performances of coating without degrading the optical performances. Titanium doped Ta_2O_5 coatings recently developed at LMA are the best solution known so far. The AdV baseline design foresees the use of mirrors, for the Fabry-Perot cavities, 35 cm in diameter and 20 cm thick i.e. mirrors having the same diameter as Virgo but twice as thick. An alternative option is to use 30 cm thick mirrors i.e. weighting 63 kg (see fig. 11). A larger mass could be interesting if the gravity gradient noise is found to be smaller than foreseen by the present model adopted within Virgo. In this case, and supposing that ribbons were used to suspend the mirrors, a heavier mirror would allow to reduce the radiation pressure noise thus improving the sensitivity at low frequency. The mirrors used for the power recycling and signal recycling mirrors will be thinner. The option considered here consists in using mirrors 35 cm in diameter and 10 cm thick. A larger substrate is likely to be required for the beam-splitter as this component lies at 45 degrees with respect to the beam axis. A substrate 55 cm in diameter and 6 cm thick has been considered (larger pieces are available if the specifications on the optical quality of the silica can be relaxed respect to what used in Virgo). The option to have a non-degenerate recycling cavity is being considered for the interferometer optical configuration. In this case the size of the beam splitter might be reduced slightly. On the other hand the implementation of such a solution will require additional large optics in the recycling cavity.

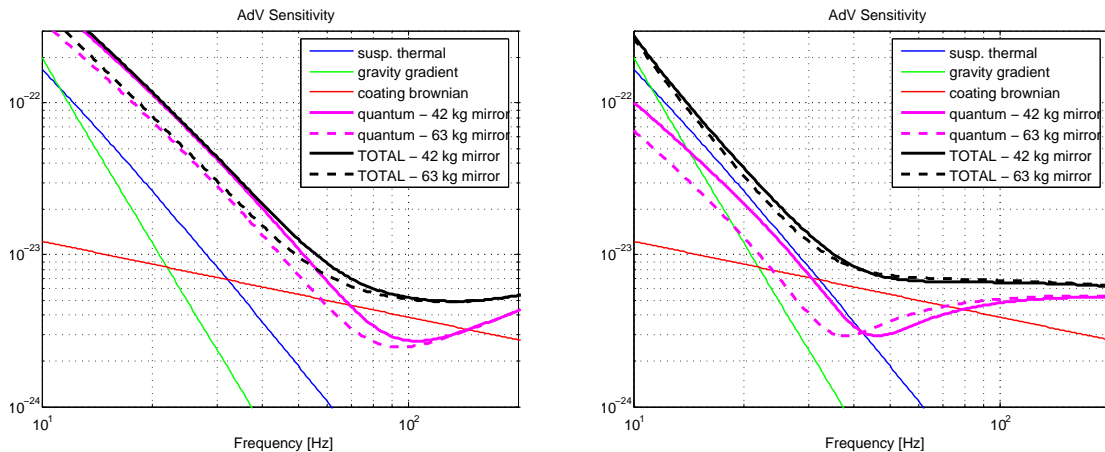


Figure 11: The reference sensitivities of fig. 2,3 (respectively without and with SR) are compared with the one obtained with 30 cm thick test masses (dashed lines).

6.1 Substrates

The AdV baseline foresees the use of fused silica for the mirror substrates. Tests on sapphire were done at LMA in the context of the Advanced LIGO pathfinder. The results obtained favored the choice of fused silica. No alternative material is being considered today by Virgo. On the other hand a new type of fused silica with smaller absorption is available today. According to the company producing it, the absorption for this material is about 5 to 10 times smaller than the one used for Virgo. The cost of this new type of Silica is comparable to the one used for Virgo. Reducing the absorption in the substrates is certainly of interest as the power absorbed causes thermal lensing in all transmissive optics. The problems increases with the power stored in the interferometer and with the thickness of the substrates. On the other hand one should remind that so far thermal effects are dominated by coating absorption, and this will be enhanced by the high finesse of AdV. From this point of view it is more important to improve the absorption of the coatings than to improve the losses of the silica. Both for the old type of silica used for Virgo as for the new one recently developed, it is possible to obtain pieces of the size requested by the AdV baseline. In the case of the fused silica used for Virgo the manufacturing of larger pieces is possible as well. In the case of the new type of silica this has to be verified. For the AdV baseline the use of an high quality fused silica (Suprasil 311 or 312 SV) has been considered for the input mirror and the beam splitter as these optics transmit a relatively large amount of power (about 2-3 kW). Fused silica of a lower optical quality is considered for the end mirrors as in this case the mirrors are reflecting most of the light. The only constraint in this case is the substrate mechanical quality factor that has to be sufficiently high to avoid increasing the thermal noise above the level determined by the mechanical losses in the coating. Fused silica of lower mechanical and optical quality can be used for the power recycling mirror as a relatively small power is transmitted through this optic and the interferometer output is less sensitive to the thermal noise affecting these masses. The same material is considered for the signal recycling mirror even if in this case the sensitivity to its internal thermal noise as a function of the interferometer optical imperfection and asymmetries will have to be studied.

6.2 Polishing

Traditionally the quality of polishing is characterized by two different parameters: the flatness and the micro-roughness. The first parameter gives the rms of the difference between the perfect surface (typically a sphere) and the actual surface as measured in by phase map interferometer (i.e. for spatial wavelengths going from about 1 mm, up to the radius of the mirror). For Virgo this parameter was measured to be in the range of a few nanometers [23, 24]. The second parameter gives a measurement of the mirror surface roughness at small scale lengths (from a few microns , up to about 1 mm). For the Virgo mirrors this parameter was found to be of the order of 0.05 nm. The distinction between these two different length scales originates in the fact that different instruments are used to measure them: both effects contribute to scatter the light from the

fundamental mode to higher order modes. They generate losses and extra noise. These polishing losses will play an even more important role in AdV due to the higher finesse of the cavities. Depending on the difference in the losses between the two cavities they could be the source of finesse asymmetry and contrast defect thus modifying the constraints on other subsystems. According to the simulation of the Virgo interferometer recently done at Nice and ESPCI, using the real mirrors maps measured at LMA, the lack of flatness represents one of the main origin of losses in the cavity. The value deduced from the simulation is ~ 250 ppm per round trip. For comparison the measured losses per round trip, as deduced from the measurement of the recycling gain, amount to 500 ppm. The additional losses measured are thought to be due to the mirror contamination (this remains to be verified). Anyhow the losses foreseen by the simulation alone exceed by a large fraction the losses assumed in the AdV baseline (~ 75 ppm per round trip). For this reason it is necessary to improve the mirror flatness. Two paths are possible in this regard. The first one consists in looking for a better polishing at the level of the mirror production. The second possibility consists in improving the mirror surface figure by using the so-called corrective coating technique. This technique, originally developed at LMA, consists in measuring the mirror surface map and correcting it by adding an additional layer of silica wherever is necessary. A R&D program about corrective coating had been supported at LMA during the first R&D program launched by EGO back in 2002. The corrective coating technique was also tested on a 150 mm diameter flat mirror with good performances (RMS wavefront: 0.9 nm, Wavefront PV: 9 nm). Further developments will require additional investment in order to improve the coater robot in Lyon. The possibilities of this technique need to be quickly characterized to understand its applicability to AdV. An effort of modeling will have to be done to understand if a given polished substrate can be used in AdV or if they should go through a corrective coating process.

6.3 Coating

The mirror coatings are certainly the most sensitive component of the mirrors and among the most important in the interferometer as they determine both the total mechanical losses of the mirrors and their optical losses. As mentioned above an R&D program is ongoing since several years at LMA. At present the lower mechanical losses measured for Ta₂O₅ coating are those obtained with Ti doped Ta₂O₅ and amount to about 1.6 to 1.8 10^{-4} [6]. It is clear that a further decrease of the mechanical losses will directly benefit to the sensitivity of the detector. For this reason the search of new materials to be used for coatings having both low optical losses and low mechanical losses should remain one of the priorities of the R&D program. One of the main difficulties in this context is to find materials with lower mechanical losses without degrading the performances in terms of optical losses. Another option to reduce the mechanical losses consists in optimizing the thickness of the different coating layers (Ta₂O₅ and SiO₂). Since the Ta₂O₅ is the more lossy material, it is possible to reduce the mechanical losses of the multi-layer by reducing the amount of Ta₂O₅ and increasing the amount of SiO₂. For a given required reflectivity it is possible to find an optimum combination. Recently at LMA a mirror was

coated using this technique and delivered to Caltech. The results should be known soon.

The absorption losses of the coatings play also an important role as they determine the power absorbed in the test mass and thus the thermal lensing effect. The lower are the losses in the coating the lower is the required thermal compensation. Since the first generation of VIRGO mirrors the absorption in the coating has been reduced. An absorption level around 0.3-0.4 ppm is done currently on high reflectivity mirrors (IM, EM) thanks to the use of Ti doped Ta_2O_5 . Nevertheless, due to the increase of the finesse, the absorption in the coating is likely to remain the main origin of the mirror heating. At the present time, we can not know if it is possible to decrease more this level of losses. R&D on coatings is needed to investigate possible paths to reduce them further. Due to the higher reflectivity of the input mirrors it will be important to check that the transmission of the two mirrors and, more critical, the losses in both arms are equal. Otherwise, the asymmetry in finesse and reflected power might be too large. Specifications for these parameters will have to be defined. In case the asymmetry is too large, then an imperfect AR coating on the other face of the substrate provides a way to improve the symmetry by tuning the reflectivity of the input mirrors. In case this is not required, 'perfect' AR and a wedge between the two faces of the substrates might be used. In both cases the specification for the AR coatings will have to be determined. In the second case the presence of larger wedges will have to be taken into account when designing the tools required both for the coating and for the metrology.

6.4 Metrology

The metrology tools, necessary to completely characterize the Virgo mirrors, have already been developed for the first mirror generation (absorption, scattering, transmission, wavefront, radius of curvature, roughness, point defect detection). Since 2002, improvements of these benches have also been obtained. The size of the AdV mirrors will impose modifications of the several sample holders to be able to map the scattering and the absorption losses, because of the weight increase. But these changes will not be too expensive. Nevertheless, the new beam configuration in the AdV interferometer should also imply the use of a larger beam splitter (diameter greater than 400 mm). This dimension will induce considerably large and expensive modifications of the metrology mirror holders. Moreover, for the scatterometer for instance, we do not know at the moment if the manufacturer (SMS) will accept to do this modification. The beam splitter will be measured at 45° incidence (wavefront of each side and transmitted wavefront). The reproducibility and the reliability will be the same as the one for the measurements at 0° of incidence (RMS reproducibility of absolute measurement lower than 1 nm).

6.5 Cleaning

During the coating process the mirrors are cleaned several times. Due to safety reasons the cleaning procedures used for Virgo cannot be simply transposed to the larger mirrors that will be used in AdV. A different cleaning procedure will have to be developed. A

new procedure has been identified by the team at LMA and its development had been already proposed in the context of the 2nd R&D program supported by EGO but not financed so far. The implementation of this new cleaning procedure will require some investment at LMA. Before being sent to the site the mirrors will have to be protected against contamination and properly packed. Special boxes adapted to the larger size of the AdV mirrors will have to be procured.

6.6 Charge buildup

It is well known that the electrical charging of fused silica samples affects its mechanical losses. A degradation of Q is correlated with the charge on the surface. On the other side the random charges stopping inside the mirror induce a shot noise effect, which depends on the absolute value of the number of charges deposited (multiplied by the Z^2) and not on the net charge itself. Electric charges accumulating in the mirror generate in-fact spurious Coulomb forces between the masses and the surrounding apparatus. This process may increment the noise level of the experiment. It is important that this effect could affect more the detector sensitivity in the case in which electrostatic actuators will be used.

6.6.1 Mirror Charge Control

The measurement of the net charge deposited on to the mirror can be performed by means of electrostatic driving electrodes facing the mirror surfaces. The charge can be measured by modulating the voltage of the electrode and measuring the coherent response at the modulation frequency of the mirror motion. Charge transfer can be then performed until the induced mirror displacement is minimized, yielding a neutralization of the charge. This charge measurement technique is conceptually easy to realize. A drawback is the difficulty in the determination of the overall mirror charge, because of the limitation of the measured charging electrodes size and distance from the mirror itself. The identification and selection of the most sensitive areas where to perform the charge measurement is a first task. Two parallel strategies can be followed to mitigate the charge accrual on the mirrors. On one side, UV light irradiation can be used to neutralize the total charge accumulated onto the mirror surfaces, when combined with a dedicated charge measurement technique. On the other side, making use of electrically conductive mirror coatings can ensure electrostatic homogeneity. Here we list characteristics, advantages and drawbacks of these two strategies.

UV light irradiation This is the technique currently used in LIGO, GEO600 and chosen for LISA. The charged mirrors are kept electrically neutral by irradiating with UV light the charged surfaces and/or the surrounding ones. Photoelectric emission produces electron currents from the illuminated surfaces, and the electrons can be then driven from one side to the other with appropriate biasing DC voltages, ensuring bipolar charge transfer. The conventional UV light sources are RF excited mercury vapour lamps and UV LEDs.

UV lamps have been largely chosen in the past as the source for irradiation, they ensure a widespread spectrum of wavelengths (tens of nm), but they show several undesired characteristics, like fragility, power instability, sensitivity to temperature fluctuations, short lifetime (hundreds of hours) and, very important, they are sources of electromagnetic interference. UV LEDs have been recently identified as an alternative source and they have been successfully tested either for LIGO and LISA. The UV LED emission efficiency ensures photoelectric emission for several kind of materials and typical lifetime is in the order of 10^4 hours. UV LEDs allow the so called AC charge transfer technique, based on the On/Off fast modulation of the UV light combined with an in phase (or out of phase) square modulation of an electric bias voltage, which allows bipolar charge transfer. This technique has been successfully demonstrated and presents several advantages compared to the standard DC technique, first of all the possibility to modulate the UV light at frequencies far from the frequency band of the gravitational wave measurements avoiding low frequency drifts and instabilities. The only disadvantage of the UV LED is the narrow spectrum of wavelengths produced by a single diode. Selection of LEDs with the desired wavelength, based on the chosen mirror coating material, must be performed and the related properties must be investigated. The advantages and the efficiency of the implementation of a charge control system based on UV light are visible. A limitation of this charge transfer technique is the fact that, if the mirror surface is not electrically conductive, charge can be removed only from the irradiated surfaces, forcing to irradiate with UV photons the all mirror surface. Also, the role of surface reflectivity, which could limit the absorption of UV photons and thus the extraction of the electrons, must be considered as well as the geometry to be chosen for the illumination of the surfaces themselves. As an alternative, one could select the mirror areas most sensibly coupled, through the charge, to the surroundings, and focus the charge mitigation only on these areas. Finally, a possible drawback comes from the impact of UV light itself on the quality of the mirror surfaces and in particular on the mirror coatings, with related possible degradation.

Mitigation of the accumulated charge Conductive coatings can help to reduced the charge accumulation on the mirrors. The provided higher electrical homogeneity sensibly reduces the role of charge patches, that can be limited down to the level of few tens of mV in the case of metallic coating. It must be noted that, in case of a non-conductive mirror, the UV irradiation only ensures the neutralization of the total charge on to the mirror, but it does not cancel the presence of single charge patches localized in small portions of the mirror surface itself. Conductivity of the mirror surfaces makes more efficient the UV discharging scheme and it makes it simpler because the portion of the mirror surface to be illuminated is sensibly smaller. Drawbacks of such a coating are a possible degradation of the mirror mechanical quality factor and simultaneously the deterioration of its optical properties. For this reason the choice of the coating material is very important to find the best ratio between the gain introduced by the surface conductivity and the limitations introduced by its mechanical losses or the optical properties.

6.6.2 Status of R&D

A study on the charge buildup has still to be started within the Virgo project. For GEO600 and LIGO great work has been performed on the UV discharging and on the conductive coating strategy. An R&D activity in the Virgo frame has to start from these experiences. Two main tasks are to be investigated:

- **Simulation approach**

A study is needed to take in account the interaction between a charged test mass with the surrounding apparatus to estimate the level of the noise that can be introduced by the charge, and to try to find a strategy to minimize its effect. On the other side it is needed to estimate the noise induced by the charge shot noise on the electrostatic actuators in case they will be implemented for AdV.

- **Measurements**

Few tasks are quite important to be investigated to have a complete overview of the charging effect on the detector and to minimize its effect. The followings are the most urgent:

- *Effect of charge on Mirror Q degradation*

It has been demonstrated that charge has a role in the mirror Q degradation, this effect induces a rubbing friction between the mirror and a piece of dust attracted by the charged sample that appears as a Coulomb damping. A facility has to be developed to directly measure this effect and to better minimize it.

- *Charge measurement and control techniques*

The charging of the masses has to be monitored to be discharged and to decrease its noise level. The geometry of the measuring system has to be evaluated to reduce the "patch effect".

- *UV light-Mirror coating interactions*

There is an indication that the UV light could damage the coating surface changing its absorption and reflectivity. A direct measurement of it is important to choose the better strategy to be followed.

- *Effect of Mirror coatings on the Q factor*

The possibility to have a conductive coating to reduce the charge effect is an open question and one of the most discriminant between this and the UV light will be the effect of a coating with these characteristics on the mechanical Q of the optics.

7 Thermal compensation

The compensation of thermal lensing due to excess absorption in the input test masses was found to be necessary in the initial LIGO interferometers, where a thermal compensation system (TCS) is in operation since 2004. Similar thermal effects have also been observed in Virgo, making the procedure to lock the interferometer more complex and preventing the ITF to work at full power. Thermal compensation will be an even more essential part of AdV, due to the much greater circulating laser power. It is, then, necessary to study a TCS to correct the thermal lensing and satisfy the noise requirements of AdV.

7.1 TCS design

The TCS will correct for a wide range of thermal effects in several optics. While R&Ds to reduce the coating and substrate absorptions are ongoing, TCS provides great flexibility for corrections in case some optics does not meet the specifications. In addition, TCS provides an online tool for correcting mirror radius errors, and can be used to suppress acoustic parametric instabilities. For these reasons, TCS should be designed with as much flexibility as possible.

7.1.1 Compensation plate

A TCS will be installed in Virgo+, based on a pre-stabilized CO₂ laser projector, that shines a heating pattern onto the HR surface of both the input mirrors. The power stabilization level, necessary to be compliant with the Virgo+ sensitivity requirements, has been estimated to be of the order of $10^{-7} \sqrt{\text{Hz}} @ 30 \text{ Hz}$ [25]. For the AdV case, detailed calculations have not been performed yet, but it is expected that the needed power stabilization level is impossible to achieve with the Virgo+ TCS scheme. If this is the case, one possible solution could be to illuminate, with a CO₂ laser projector, compensation plates (CP) placed into the recycling cavity. Since CP live entirely within the recycling cavity and have no HR surfaces, the effect of the actuator noise is much less important on a CP than on a test mass. The disadvantage of the compensation plate is that it cannot compensate errors within the arm cavities. Calculations of the noise coupling of the CP have been performed [26] and show that the power stabilization level required would be of the order of $10^{-6} \sqrt{\text{Hz}} @ 100 \text{ Hz}$, less stringent than the Virgo+ case, due to the smaller noise coupling. The reasons to prefer a CO₂ laser projector instead of a heating ring to heat the CP are:

- CO₂ laser projector can compensate non-axisymmetric thermal lensing;
- Most of the apparatus lives outside vacuum and can be easily upgraded as new understanding of the ITF is realized.

The CP interacts directly with the interferometer beam. As such, it must satisfy requirements like those of a core optics with respect to displacement noise, absorption and

scattering, index homogeneity, antireflection coatings, and the like. In particular, we are aware that multiple reflections of the main ITF beam could occur between the ITM and the CP. A possible solution, that we are evaluating, to mitigate this effect, could be to add a wedge to the CP and a baffle of annular shape on the back side of the CP (i.e. looking toward the recycling cavity). This is only one possibility, this is indeed a very delicate issue and it must be investigated more deeply. The CP isolation requirements are less stringent than those for the input mirrors, so suspending it from the input mirrors reaction chain should provide enough isolation. The design of the last stage of the superattenuator should take into account this possibility.

7.1.2 Test mass shielded ring heaters

While CP will only compensate thermal aberration effects in the recycling cavities, it is necessary to study a solution to compensate thermal effects in the Fabry-Perot cavity. The self-heating of the test masses will be predominantly through absorption in the HR coatings. This will deform the whole optics, making its surface profile nonspherical and thus reducing the radius of curvature. The Fabry-Perot cavity becomes less concentric, and the spot sizes at the mirrors will shrink. The resulting increase of thermal noise has been estimated to be of the order of 15% [27]. However, this deviation from sphericity could not make the arm cavity resonant modes significantly non-Gaussian. But it could be necessary to control the radii of curvature of all test masses. Compensation and control of the test mass HR surfaces could be done by shielded ring heaters, suspended from the last stage of the superattenuator or embedded into the reference mass. There would be four of these: one around each test mass, toward the AR face. The test mass ring heaters would control the arm cavity mode shape. The input mirror ring heaters could also provide limited compensation of thermorefractive aberration in the recycling cavities. The test mass ring heaters might also be used to temperature-tune away radiation-pressure parametric instabilities. This design is less sensitive to actuator noise fluctuations than designs that heat the HR surface, because the heating is entirely on the substrate far from the ITF beam, and the radiation pressure averages to zero over the test mass. However, there is a slight coupling of overall power fluctuations to HR surface displacement. A test mass ring heater changes the radius of curvature of a test mass's HR surface by flexing the mirror. Since the position of the centre of the HR surface relative to the test mass centre of gravity varies with the flexure, any power fluctuation in the ring heater will create displacement noise [26]. The ring heater thermal inertia will passively smooth power fluctuations on its input supply, this should make easier to meet the noise requirements. Detailed calculations are in progress. The ring heater can compensate also for thermal aberrations in the recycling cavity, as demonstrated by Ryan Lawrence, thus avoiding the use of CPs and CO₂ laser projectors. But it cannot compensate at the same time for thermal effects in the Fabry-Perot cavity, thus inducing an increase of thermal noise.

7.1.3 TCS sensors

Each piece of optics with a significant thermal load should be independently monitored. The HR face of each test mass could be monitored in reflection for deformation. The input mirror/CP phase profile could be monitored on reflection on-axis from the recycling cavity side using a Hartmann sensor. On-axis sensing would require that the probe beam enters the recycling cavity through a pickoff port, such as the wedged AR face of the beamsplitter. The group led by Jasper Munch at the University of Adelaide, Australia, has been developing a Hartmann sensor for the Gingin experiment and as a potential wavefront sensor for Advanced LIGO. This latter device has been demonstrated to have adequate precision for Advanced LIGO and is described in the following. A Hartmann sensor is simply a CCD camera with a multiple-aperture mask between it and an incident optical wavefront. The light spills through the apertures in the mask and falls upon small clusters of pixels on the CCD. As the wavefront of the incident beam varies, so does the propagation direction of the incident light through each aperture, and the light falls upon a slightly different cluster of pixels. The sensitivity is a function of such parameters as pixel size, individual pixel sensitivity, aperture size and spacing, and the distance from the mask to the CCD. A Shack-Hartmann sensor replaces the aperture mask with a lenslet array that focuses the beamlets onto the CCD. It is more efficient with incident light but more difficult to align. The University of Adelaide's Hartmann sensor [28] has been demonstrated to have a shot-to-shot reproducibility of $\lambda/580$ at 635 nm, which can be improved to $\lambda/16000$ with averaging, and with an overall accuracy of $\lambda/6800$. The use of the Adelaide Hartmann sensor in AdV is desirable.

7.1.4 Beam splitter compensation

At present, it is not known if the beamsplitter will need to be directly compensated. If it is found that its contribution to thermal lensing in the recycling cavities is small, its effect could be compensated by the compensation plates. However, the option to directly apply thermal compensation onto the beamsplitter should be maintained in the AdV optical layout.

7.1.5 Higher order modes

As pointed out in J.Y.Vinet work [29], the use of higher order modes would reduce the amount of thermal lensing in all test masses with respect to the TEM₀₀ case. Yet detailed calculations must be performed to determine how the residual thermal aberrations will affect AdV sensitivity and operation. Reduced thermal lensing could ease the design and operation of the TCS, as less power must be injected on to the test masses. Thus, power stabilization requirements become less stringent, increasing the number of possible solutions that can be adopted for the TCS.

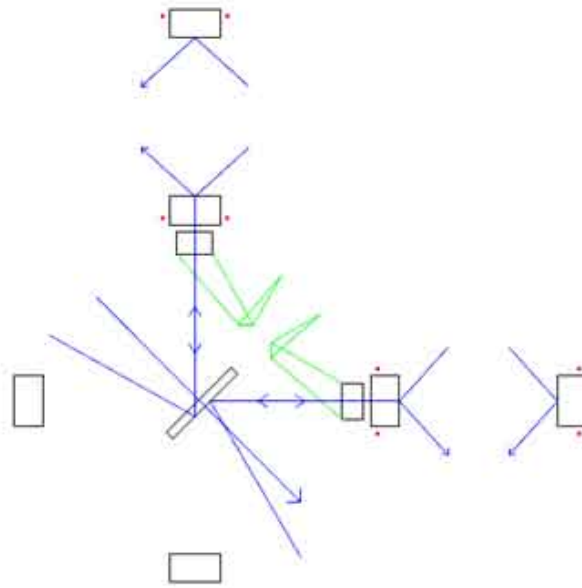


Figure 12: AdV TCS layout under study: the red dots represent the test masses shielded ring heaters, the green rays represent the CO₂ laser beams acting upon compensation plates, the blue lines represent the sensing beams.

7.1.6 A possible scheme

Figure 12 shows a possible scheme of the AdV TCS using both CO₂ lasers and heating rings.

7.1.7 Status of the related R&D

An intensive R&D program must start as soon as possible, since there are a number of questions that need to be answered, such as:

- magnitude of the lensing effect into AdV test masses;
- whether or not the BS needs compensation;
- power needed to fully compensate thermal aberrations;
- power stabilization level for the TCS to be compliant with AdV sensitivity requirements;
- build and test a prototype of the TCS, in an environment that reproduces the distribution of masses inside AdV towers;
- test the quality of the compensation achieved using Hartmann sensor.

8 Detection system

The upgrades to the detection system depend on the interferometer parameters. The photodiode electronics will have to be redesigned if the modulation frequency is changed. It might anyway be needed to produce new electronics in order to ensure more flexibility and spare boards. In the case of DC readout the dark fringe photodiodes should be changed since it is possible to work with larger photodiodes and therefore to reduce the sensitivity to environmental noise. The case of Signal Recycling (SR) has not been studied yet but the detection system should be flexible enough to work with or without the signal recycling strategy.

8.1 DC detection and needed modifications

In the DC readout scheme a small offset is added to the dark fringe working point so that the DC channel of the dark fringe is sensitive to the gravitational wave signals. The arm's differential control is switched from the demodulated signal to the DC signal. The DC control has already been tested successfully in GEO and LIGO. *In the following only the case without SR is discussed.*

The main advantage of the DC readout is a smaller (about 20%) shot noise with respect to the AC readout. There are also advantages for technical noises:

- There is no demodulation noise which is usually one of the dominant source of noise at high frequency for the AC readout.
- There is also no frequency noise due the asymmetry of losses into the Fabry-Perot cavities which is also one of the limitations for AC readout at high frequency. The frequency noise due to finesse asymmetry is the same as in the AC readout case [30].
- Larger photodiodes can be used since no demodulation is needed.
- The problem of reduced spatial overlap between the carrier and the sidebands is also not present with DC readout.

The drawback of DC readout is an increased laser power noise coupling:

- The carrier power noise is filtered by the double cavity pole which should be around few Hz for AdV so that it is an issue only for low frequencies (typically below 100 Hz).
- The sidebands should be removed from the dark fringe by means of the output mode cleaner so that their contribution to the dark fringe is small enough (less than few %) and they do not increase the shot noise. Even with a small sideband contribution, since the power noise of the sidebands is not filtered by the double cavity it can be a limitation at high frequencies.

More details on technical noises in the case of AC or DC readout can be found in [30].

8.1.1 Power noise considerations

- **Carrier noise:** The DC power on the dark fringe is given by:

$$P_{\text{car}} = \frac{P_0 G}{2} \left[(1 - C) + \frac{1}{2} \left(\frac{8\mathcal{F}}{\lambda} L_{\text{off}} \right)^2 \right] \quad (1)$$

where P_0 is the input power, G the power recycling gain, C the contrast, \mathcal{F} the finesse, L_{off} the offset. The offset should be tuned so that the contribution of the contrast defect is small enough. Assuming a contrast defect as good as for Virgo (few 10^{-5}) and given the high finesse of AdV (~ 1000) an offset as small as $5 \cdot 10^{-12}$ m could be used. This offset also has to be kept well above the locking accuracy (it is of the order of 10^{-13} m in Virgo). The offset should not be too high in order to keep the carrier power noise under control: the power noise increases quadratically with the offset while the optical gain only increases linearly.

In Virgo the power is stabilized after the input mode cleaner using a photodiode located under vacuum. However the power noise observed in the interferometer (B5 photo diode) is relatively high at low frequencies (below 50 Hz) due to the noise introduced by the control loops (the power recycling longitudinal control in the Virgo case). It seems therefore necessary that the power stabilization uses as error signal a measurement of the power stored inside the recycling cavity (B5_DC) for the low frequency part (below 50-100Hz). Using B5 for the power stabilization will imply to seismically isolate these photodiodes and to put them under vacuum. At higher frequency, due to the filtering of the double cavity the B5 measurement will be shot noise limited and therefore the power stabilization should remain the same as for Virgo (using the photodiode just after the IMC).

- **Sidebands noise:** The sideband power on the dark fringe is given by:

$$P_{SB} = 2P_0 T_{SB} \left(\frac{m}{2} \right)^2 T_{OMC} \quad (2)$$

where T_{SB} is the transmission of the sidebands to the dark fringe which depends on the Schnupp asymmetry, T_{OMC} is the output mode cleaner transmission for the sidebands and m is the modulation index. Smaller modulation depth reduces the sideband amplitude. The transmission of the output mode cleaner for the sidebands should be kept typically below a few %. For a given output mode cleaner, increasing the modulation frequency reduces the sidebands transmission. Increasing the modulation frequency with respect to the Virgo case will therefore reduce constraints on the AdV output mode cleaner.

8.1.2 Requirements

To obtain some quantitative requirements on the carrier and sidebands power noise the following ITF parameters have been used (no SR case, derived from [5]): $L_{\text{off}} = 8 \cdot 10^{-12}$ m, $P_0 = 125$ W, $\mathcal{F} = 880$, $G = 23$, $T_{SB} = 7\%$, $m = 0.15$, $T_{OMC} = 3\%$. With these parameters

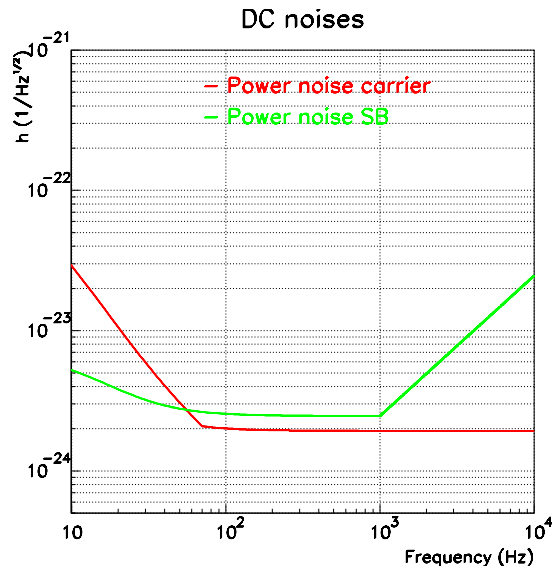


Figure 13: Contribution of sidebands and carrier power noise to AdV sensitivity under the assumptions made in the text (without SR).

the power on the dark fringe is 1.8 W out of which 3 mW arise from the sidebands. If a smaller offset can be used (depending on the locking accuracy and the sidebands power noise) the power on the dark fringe can be well reduced (it goes quadratically with the offset). The sideband transmission assumes the same geometrical configuration as for Virgo and the same modulation frequency.

The Virgo sideband's power noise is limited by modulation amplitude noise above ~ 50 Hz and by PR longitudinal control noise below. It is assumed that these noises are reduced by a factor 3 (the modulation electronics can be improved and the PR control as well) but remain above $3 \cdot 10^{-8}$.

For the carrier it is assumed that the power can be stabilized at the level of $2 \cdot 10^{-8}$ at 10 Hz, $4 \cdot 10^{-9}$ above 60 Hz with a $1/f$ dependency from 10 to 60 Hz. To achieve this performance it will be necessary to use B5_DC as error signal below 50-100 Hz and to place the B5 photodiodes under vacuum.

Under these assumptions the power noise contribution to the AdV sensitivity is shown in Fig. 13 (without SR). Details about this computation can be found in [30]. One can rescale these noises with the ITF parameter knowing that:

- the contribution of the carrier power noise varies proportionally to L_{off}
- the sidebands power noise contribution varies proportionally to $1/L_{\text{off}}$, m^2 , T_{SB} , T_{OMC} , $1/G$, $1/\mathcal{F}^2$.

8.1.3 Status of the related R&D

- **Output mode cleaner under vacuum** An output mode cleaner with the same geometry as the Virgo mode cleaner is being developed by the LAPP and LMA groups: a triangular monolithic cavity of 2.5 cm. The aim is to increase the finesse up to about 1500 in order to reduce the transmission of the sidebands down to 3% for $f_{\text{mod}}=6$ MHz. If it is validated it could be used for Virgo+ without any modification of the detection bench. It could then also be used for AdV. The beam jitter noise could be a problem and still has to be estimated. Thermal effects are also a worry and will be measured on the prototype. To keep the total losses below 1% the new mode cleaner is made of Suprasil and the polishing should meet a roughness below 2 Angstrom. Two silica blocks have been produced and polished and one will be coated soon (end of 2007). If this technology does not work a larger non-monolithic mode cleaner will have to be developed. A possibility is to use a similar mode cleaner as the one developed for the Virgo+ pre-mode cleaner.
- **Photodiodes under vacuum** In order to be isolated from seismic and acoustic noise the photodiodes will be located on the suspended detection bench. A system to monitor and remotely control the alignment will be implemented. This system is under development at LAPP.
- **Power stabilization** The Nice group will take care of the R&D concerning the DC power stabilization.

9 Optical design

9.1 Signal recycling

The signal recycling technique (also known as dual recycling) consists of adding a new mirror, the signal recycling mirror (SRM), at the output port of the interferometer. This mirror together with the Michelson interferometer builds up a new cavity, the signal recycling cavity (SRC). Basically, if the SRC is made resonant for a GW sideband frequency, there is an enhancement in the response of the detector at this frequency. This enhancement depends on the SRC finesse, hence on the SRM reflectivity and the shape of the enhancement (as a function of signal frequency) can be changed during operation by changing the so called *tuning* of the SR, which is determined by the microscopic positioning of the SRM. The drawback of SR is a narrowing in the detector bandwidth as well as introducing an additional complexity by the extra mirror and its influence on the resonance conditions for RF sidebands.

The SR technique is already implemented in the GEO 600 interferometer and is foreseen to be implemented in Advanced LIGO. Therefore these detectors will have the ability to change the shape of their sensitivity curve online by tuning the SRM. It might be advantageous for a common data analysis if Adv provides the same technique so that the detector responses can be optimized with respect to each other.

9.1.1 Quantum correlations

The SRM further induces a coupling of the output port of the interferometer with the radiation pressure fluctuations [31]. A simple estimation of the order of magnitude shows that these effects can not be neglected for advanced detectors. If we consider for example the Standard Quantum Limit (SQL),

$$h_{SQL}(\Omega) = \sqrt{\frac{8\hbar}{mL^2\Omega^2}}, \quad (3)$$

where m is the mirror mass and L the arm length, we find numerically for $m \simeq 30$ kg and $L \simeq 3$ km, $h_{SQL} \simeq 3 \times 10^{-24}$ Hz^{-1/2} at $\Omega = 2\pi \times 100$ Hz. Advanced detectors are likely to approach such sensitivities.

Figure 14 displays an example of quantum noise spectral density obtained with the following parameters : $SRM_r = 0.9$, the SRC half width $\gamma = 2\pi \times 122$ Hz, hence a arm cavity finesse around 200, a laser power I_0 matched to $I_{SQL}(\gamma)$, hence the power impinging on the beam splitter being $I_0 \simeq 13$ kW (compatible with a 100-200W input laser power).

The SR technique can improve the overall sensitivity of the instrument only at frequencies where the optical quantum noise is supposed to be dominant. By proper choice of the optical parameters SR allows for a significant improvement of the quantum noise in a frequency band around the peak sensitivity. As figure 14 indicates with SR it is even possible to achieve a quantum noise level below the SQL.

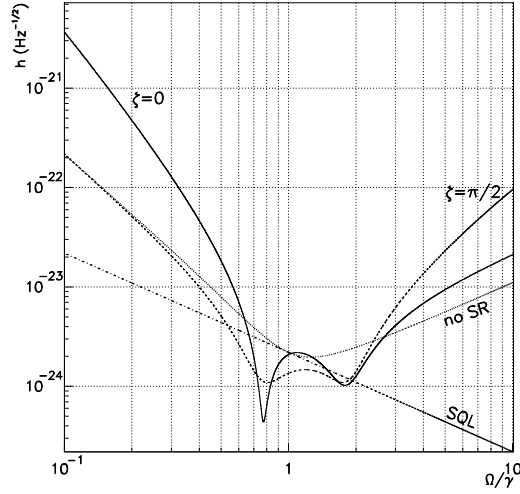


Figure 14: Sensitivity of a dual recycled interferometer (quantum noise only). The two quadratures are displayed. The SQL is also shown as well as the Power Recycled interferometer sensitivity (no SR). The PR interferometer sensitivity reaches the SQL at $\Omega = \gamma$, as expected from the parameters choice while both quadratures give sensitivities locally below the SQL.

9.1.2 Other connected changes and side effects

In principle, no major infrastructure change is required in order to install the SRM since the base of the vacuum tank for the SRM is already integrated in Virgo. Nevertheless the SR tower must be provided with a Superattenuator chain and its related local controls and electronics. Other changes are needed for the control chain itself. Extra modulation frequencies are likely to be needed for locking and alignment. This means new modulators and demodulation boards and extra photodiodes. If extra modulation frequencies are effectively used, a change in the input benches is then needed: a Mach-Zender interferometer with an EOM in each arm will be required to avoid the problem of the sidebands of sidebands as shown at the Caltech 40m prototype. An update of the detection bench may also be required mainly for a change of matching optics (depending in particular on the SRM curvature radius choice).

A beneficial side effect of SR is that it helps to filter “bad” light, i.e. spurious high-order modes generated by interferometer mirror aberrations. The net effect is an improved interferometer contrast that allows to relax the mirror specifications [32, 33].

9.2 Degeneracy of recycling cavities

The baseline design of AdV foresees the use of degenerate power recycling (PRC) and signal recycling cavities (SRC). As it is known degenerate cavities, if mirrors aberrations

are present, extract power from the fundamental mode by the coupling with high order modes. This can significantly reduce, in particular, the amplitude of the TEM₀₀ component of the radio frequency (RF) sidebands in both, PRC and SRC, and the amplitude of signal sidebands in SRC.

The effect of mode coupling has been observed in Virgo (and in LIGO) due to thermal deformation of the input mirrors: in steady state the relative amplitude of the first Laguerre mode with respect to the fundamental (measured as a mean of the two sidebands) is approximatively 0.3, resulting in a reduction of the recycling gain. While the operation of the first long science Virgo run has not yet seen the necessity of operating a compensation of these effects, AdV could face more serious problems due to its higher light levels. D'Ambrosio [34] and successively Pan [35] have shown that if the signal to noise ratio of Advanced LIGO should not be reduced by more than the 1 percent due to mode mixing, the peak-to-valley surface distortion of the mirrors (in their central region) in the SRC must be less than 1 to 2 nm. Similar results apply to AdV which requires the use of a thermal compensation system. Such a system is presently being built; it will be installed and commissioned within Virgo+ and will be used also for AdV.

Nonetheless a possible relaxation of the constraints of the mirror aberration could be obtained using non-degenerate PR and SR cavities. This condition is satisfied if the frequency distance between the fundamental and higher order modes is larger than the resonance width $\Delta\nu_C$. A useful way to write the frequency difference between any higher Hermite-Gauss mode and the fundamental makes use of the cavity's Guoy phase η , related to the cavity's g -factor by: $\eta = \arccos \sqrt{g}$. (For a cavity of length L and mirrors radii R_1 and R_2 and $g_i \equiv 1 - \frac{L}{R_i}$). It is also useful to remember that the Guoy phase $\eta(z)$ for a Hermite-Gauss beam at a distance z to the waist is given by: $\eta(z) = \arctan\left(\frac{z}{z_0}\right)$ where $z_0 = \frac{\pi w_0^2}{\lambda}$ is the Rayleigh length.

In order to obtain a non-degenerate cavity η must be sufficiently different from zero and this can be obtained if the length of the cavity L is larger than the Rayleigh length. More precisely the Guoy phase corresponding to a frequency shift $\Delta\nu$ must satisfy

$$\Delta\nu = \frac{c}{2\pi L}\eta > \Delta\nu_C. \quad (4)$$

If this condition is satisfied the higher order modes generally do not resonate except for those modes that have a Guoy phases (*mod* 2π) close to zero. These modes have typically very high orders and are strongly suppressed by diffraction losses.

The Rayleigh length of the laser beam in AdV will be of the order of 500 m so that the long-arm cavities can be easily not-degenerate. Instead the lengths of PRC and SRC will be 6 m so that it is not possible to design them in order to be not-degenerate. In particular the frequency shift of the cavity will be few kHz, far less than the bandwidth of the PRC $\Delta\nu_{PRC} \approx 100$ kHz.

Following these consideration we observe that the reduction of Rayleigh length or/and the increases of the cavity lengths could allow to remove the degeneracy. These two possibilities are currently under study, especially for Advanced LIGO [36]. From a practical point

of view PRC and SRC degeneracies could be removed by inserting the input telescope for beam matching inside the interferometer, and a second telescope inside the SRC, as shown in figure 15 (Using only a single lens is not sufficient for giving a proper Guoy phase in neither the PRC nor the SRC).

Another possibility, first suggested by Mizuno [37], is to use a 3 km long SRC to collect power in both signal sidebands and increase the signal-to-noise ratio by a factor of 2. A possible design is reported in figure 16. At the moment such studies are being developed also within Virgo to better understand the actual feasibility.

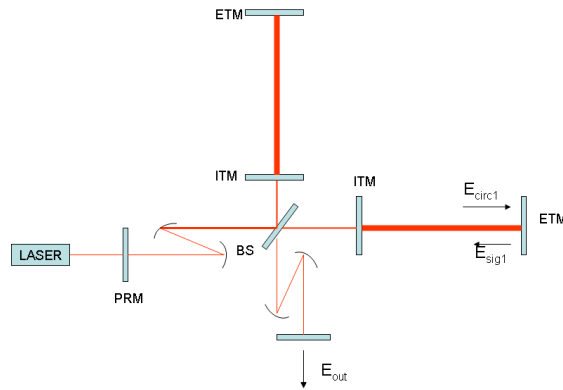


Figure 15: AdV with telescope in short cavities

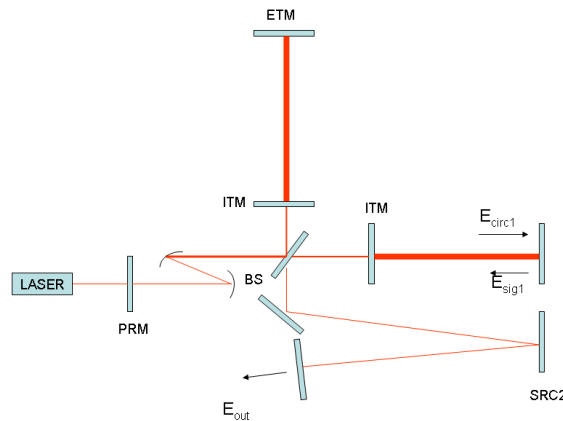


Figure 16: AdV with telescope in PRC and 3 Km SRC

9.3 Wedges and pick-off beams

In the current Virgo optical layout, the core optics have no wedges (apart from the central beam splitter). It is under consideration to have wedges on (at least) the input mirrors of the arm cavities. First of all, if the input mirrors feature no wedge, the so-called etalon effect will, if it is not controlled, influence the finesse of the arm cavities. This could result

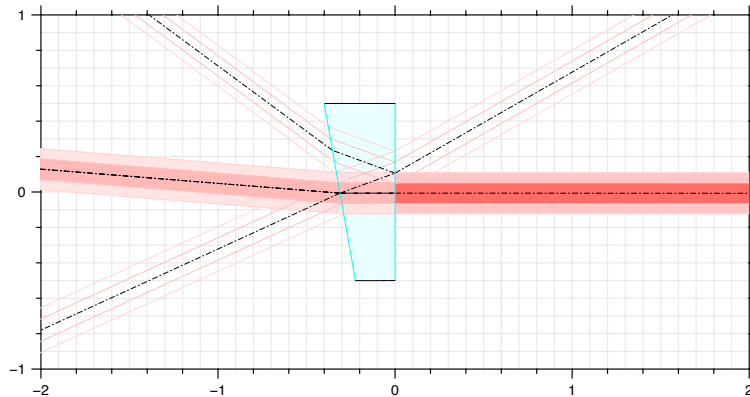


Figure 17: Extra beams generated by a wedged mirror

in a reduction of the instrument's stability. On the other hand, if the etalon effect is controlled by a servo, this might give advantageous flexibility for a DC detection system. A trade-off analysis with respect to the etalon effect has to be performed.

In addition, with wedged mirrors it would be possible to increase the number of potential pick-off beams for optimizing the sensing and control performance. Based on this motivation, one can specify the value and orientation of the wedges for each mirror in order to deliver a complete optical layout. In principle, three extra beams of interest (i.e. with sufficient optical power to be taken into account) are generated by a wedged second face of a mirror (see Fig.17). We will further refer to the extra beams as *pick-off* beams.

If the layout of the interferometer infrastructure is going to be kept we get the following constraint: it must be possible to separate the pick-off beams from the main beam and from each other in the range of 3 m (corresponding to the half distance between two vacuum towers) in order to dump them or redirect them on some sensing device. A minimum separation distance between the extra beams and the main beam of 300 mm, 2 m far away from the mirror can be achieved by a wedge of about than 52 mrad (3 degrees).

Furthermore a wedge will tilt the beam axis (see Fig.17). Assuming that the optical axis in the 3 km arms remains unchanged, a 3 degree wedge in the input mirrors corresponds to a necessary shift of the position of the central beam splitter (in particular but not only) by approximately 15 cm. This shift can obviously be in the horizontal plane as well as in the vertical plane depending on the orientation of the wedges.

A complete optical layout design is under progress to deliver the detailed specifications: new positions of the center of the mirrors and of the suspended benches, geometry of the core optics (thickness, wedge, tolerances).

9.4 Beam size and geometry

The size and shape of the laser beam inside the interferometer is defined by the surface shape of the cavity mirrors. Current detectors use Gaussian beams, resonating in *spherical cavities*. We call spherical cavities Fabry-Perot resonant cavities involving spherical mirrors in the wide sense (including flat mirrors). The theory of spherical cavities has been extensively developed and treated in laser physics books [38], and it is well-known that provided some stability conditions are satisfied, light can be stored in such cavities, which is a key argument for using such configurations in IGWA's, in order to increase the effective length of the arms.

The mathematical physics analysis of stable cavities in the limit of paraxial diffraction theory leads to families of orthogonal optical eigenmodes having three quantum numbers, one longitudinal related to phase tuning, and two related to the transverse structure of the optical beam. Two particular families of modes are currently considered, namely the Hermite-Gauss family and the Laguerre-Gauss family. The TEM_{00} classical mode is the *fundamental* of both families.

9.4.1 The TEM_{00} mode

Current GW detectors use pure TEM_{00} modes. Valuable experience has been gained in the production and handling of such beams in a high precision measurement. Thus they represent the baseline for AdV.

However, the size and position of the beam waist inside the interferometer can be chosen freely within some limits. Especially the size of the beam waist can have a direct impact on the detector sensitivity by determining the coupling of mirror thermal noise into the optical signal. The following paragraphs will motivate the need for large beam sizes and will discuss further the alternative option to use 'exotic' beam shapes to further reduce the coupling of thermal noise.

Thermal noise It has been shown that the Brownian motion of matter in the bulk material of the mirror substrate causes a specific noise, *mirror thermal noise*, whose overall level and spectral contents depends on the spatial distribution of the light power on the surface of the mirror. This contribution to the overall noise budget is predominant in the strategic region of 100 Hz. Furthermore the thermal loading of the mirrors and beam splitters due to absorption in the bulk or coating material causes distortions of the reflected and transmitted fields. Again this effect is subject to the spatial distribution of the light power.

Further, it has been shown [39] using the fluctuation-dissipation theorem that the low frequency tail of thermal noise amounts to compute the strain energy U stored in the substrate undergoing a pressure distribution having the profile of the readout beam, and

normalized to 1 N, according to the formula:

$$S_x(f) = \frac{4k_B T}{\pi f} \phi U \quad (5)$$

where ϕ is a loss angle. Computing U is more or less difficult, depending on the mode structure and on the mirror's shape. If the mirror is assumed circular and the mode centered, analytical calculations are possible.

A first formula has been given in [40] in the case of an infinite mirror (acceptable simplification if the light spot is small compared to the mirror diameter, but questionable otherwise) for a fundamental gaussian mode :

$$U_{0,0} = \frac{1 - \sigma^2}{2\sqrt{\pi} Y w} \quad (6)$$

where σ is the Poisson ratio, Y the Young modulus of silica. This makes clear that the width parameter must be as large as allowed by diffraction losses. In fact, as a simple rule of thumb the thermal noise contribution can be approximated as being inverse proportional to the beam size.

Here we focus on possible ways to reduce the contributions of thermal noise by increasing the beam size (baseline) and by using 'exotic' beam shapes (alternative option).

Sensitivity improvements In the most prominent frequency region around 100 Hz the sensitivity of AdV will probably be limited by thermal noise of the mirrors and the coatings. Increasing the beam size (assuming large enough mirrors) can reduce the thermal noise such that the quantum noise of the light becomes the limiting noise. The shape of the quantum noise depends critically on the reflectivity but also on the tuning of the Signal Recycling mirror, of which the latter can be changed during operation of the detector. Thus a comparison between thermal noise and quantum noise cannot be given easily. However, figure 3 can provide some indication: if the thermal noise could be reduced by a factor of four its effect could be eliminated from the total noise budget. Thus, if all other parameters remain the same, the largest useful increase in beam size would be by a factor of four. This clearly indicates that the beam size should be as large as possible, limited by the available size of the optics.

Beam waist position In order to minimize the influence of thermal noise, the beam spot size on the arm cavity mirrors should be maximized. This suggests to use symmetric arm cavities with equal radius of curvature of both mirrors which results in a beam waist position in the center of the cavities.

The limits for the beam size come from constraints on the optical losses. If the beam has a finite intensity at the edges of the optical component (or at the edge of the HR coating), the optical losses will at some point increase above a tolerable level.

The spot size on the mirror is given by the radius of curvature of the mirrors as shown in figure 18. This shows that the minimum spot size (for a 3 km cavity) is around 32 mm

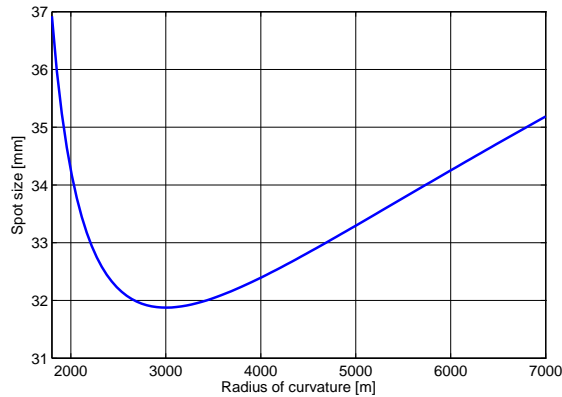


Figure 18: Beam spot size on the arm cavity mirror as a function of the mirror radius of curvature (for a symmetrical, spherical cavity of length $L = 3$ km and a laser of wavelength $\lambda = 1064$ nm).

while in principle the upper limit is given by the mirror size, see below. However, research into the length sensing and control of Advanced LIGO has shown that the Gouy phase of the arm cavities and thus the radius of curvature of the mirrors are important parameters to be optimized for the generation of proper control signals.

Beam size versus mirror size If a beam reflected by a mirror has a non-zero amplitude at the edge of the mirror, some power will be lost due to *clipping*. It can be shown that a mirror with a diameter of typically five times the beam radius of a Gaussian TEM_{00} mode causes approximately a power loss of 1 ppm due to the clipping effect. Including a further safety factor the mirrors should generally be chosen to be at least six times as large as the beam radius (this number holds for TEM_{00} only).

Another constraint is coming from the fact that the laser beam is incident on the main beam splitter under 45 degrees, and depending on the substrates thickness is positioned off-center on its back surface. Thus the minimum size of the beam splitter coating must be larger by typically a factor of 1.5.

9.4.2 Higher Order Laguerre Modes

In addition to merely increasing the size of the laser beam, we can imagine another purely optical solution to this issue, based on changing the beam profile from classical (TEM_{00}) to *exotic* profiles.

Higher order modes have the property of a wider distribution of light power on the optical surfaces. This is a reason to guess that thermal noise could be reduced when operating with such modes. We focus on The Laguerre-Gauss (LG) family because it is well adapted to polar coordinates that are obviously more convenient when considering axisymmetrical mirrors.

The LG family The spatial extension of a LG beam can be estimated through the spatial standard deviation (SD) (borrowed from statistics) with respect to the beam axis. It can be computed [41] from its width parameter w , from its azimuthal quantum number n and from its radial quantum number m :

$$\text{SD} = \langle r^2 \rangle^{1/2} = w \left(m + \frac{n+1}{2} \right)^{1/2} \quad (7)$$

For any given quantum numbers (n, m) , there exists a width parameter w that yields a set clipping loss level. For instance using a 35 cm diameter mirror, the w giving 1 ppm loss for $(0, 0)$ is 6.65 cm leading to a SD of 4.7 cm. For $(2, 2)$ we have $w=4.52$ and the SD is 8.5 cm. For $(5, 5)$ we have $w=3.5$ cm but the SD is 9.9 cm, more than twice the fundamental and seven times the SD on the Virgo input mirrors. It therefore makes sense to investigate High order Laguerre-Gauss modes (see fig. 19).

Non-spherical cavities The most homogeneous distribution of light power would be perfectly flat, falling to zero exactly at the edge of the mirror. Diffraction theory tells us that such modes would have very bad propagation properties. It is however possible to approximate such profiles.

The first proposed model [42] consists in superimposing elementary fundamental gaussian modes of given parameter w at their waist, and having axes uniformly distributed on a disk of given radius b_f . It is easy to compute the propagated mode and the resulting wavefront. The mirror matching such a mode must have the same profile, and the authors call it *Mexican hat* (*bottle bottom* would be more appropriate, see fig. 20).

For some calculations, it is possible to approximate the Mexican mode by a simple flat distribution of radius b , we call it *flat top*. It is optically wrong but sufficient for some thermal considerations.

Thermal noise The formula 6 has been extended in [43] for any LG mode (n, m) :

$$U_{n,m} = \frac{1 - \sigma^2}{2\sqrt{\pi}Yw} g_{0,n,m} \quad (8)$$

where $g_{0,n,m}$ is a numerical factor given in [43] that can be approximated by:

$$g_{0,n,m} \approx (2m + n + 1)^{-1/2} \quad (9)$$

for (n, m) not too small. In the case of a flat top mode, we have:

$$U_{n,m} = \frac{8(1 - \sigma^2)}{3\pi^2 Y b} \quad (10)$$

but the result is questionable, relying implicitly on a small ratio b/a (a being the mirror radius).

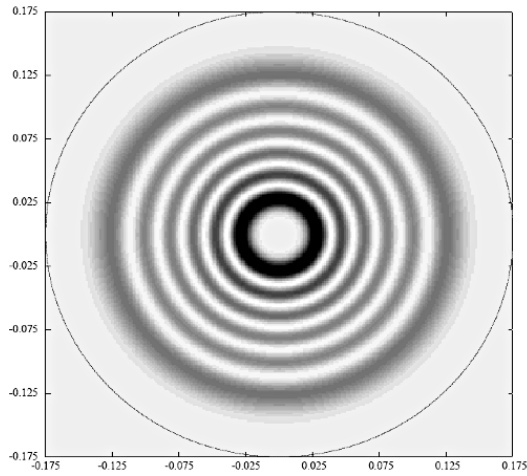


Figure 19: Intensity pattern of an axisymmetrical LG55 having 1ppm clipping losses. The thin line is the mirror edge.

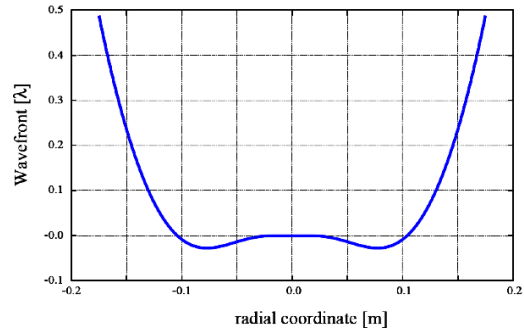


Figure 20: Wavefront of a *Mexican Mode*.

Finite mirror size A method has been given in [40] for computing U in the case of a cylindrical mirror of radius a and thickness h , centered on the beam. To be specific, some numerical examples [44] can be given. With respect to the current situation in the Virgo input mirror, a Mexican mode having 1 ppm diffraction losses would improve the sensitivity at 100 Hz by factor of about 3, whereas a LG55 mode having the same diffraction loss would provide a factor of about 5. This is why using High Order Laguerre-Gauss Modes (HOLM) deserves some attention.

Thermal lensing It follows naturally that exotic profiles are good also regarding spurious thermal effects that are already disturbing in the present antennas, and promise to be even worse in advanced systems where high optical powers are planned. The light can be dissipated at the level of the coating for intracavity stored power, and in the bulk substrate for incoming light. Dissipated power is a source of heat, and temperature gradients give rise to a thermal lens in the mirror substrate. Calculations [43] show that both channels have very close results for equal absorbed powers. For being specific, the thermal focal length is $337 \text{ m} \cdot \text{W}$ for Virgo input mirrors, assuming a temperature index of $1.1 \cdot 10^{-5} \text{ K}^{-1}$. For a mexican beam this could be increased to about $10 \text{ km} \cdot \text{W}$, and even for a LG55 mode to $30 \text{ km} \cdot \text{W}$. This means that thermal lensing is reduced by almost two orders of magnitude.

Thermal distortion The temperature gradients also cause distortions of the substrate changing the curvature radius of the reflecting surface. The calculations have been made in [43]. In terms of curvature radii, the effect is much weaker than the thermal lensing, but it affects the field inside the cavity, and also the sidebands which are not stored. Still with respect to present Virgo input mirrors ($22 \text{ km} \cdot \text{W}$), we have for the Mexican mode

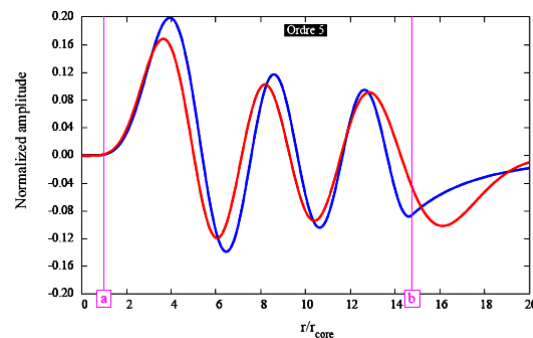


Figure 21: Comparison of a LP55 fiber/cladding mode (yellow) and a LG55 mode (cyan) (electrical field, arbitrary units).

about $324 \text{ km}\cdot\text{W}$ and $937 \text{ km}\cdot\text{W}$ for the LG55.

Thermoelastic noise Thermodynamic fluctuations of temperature in the bulk material couple to internal motion via the thermal dilatation constant. This effect results in an extra contribution to thermal noise, this has been pointed out in [45], and the calculation for exotic modes done in [43]. With respect to the present Virgo input mirrors, we have a reduction factor of about 6 for the Mexican mode, and of 5 for a LG55.

Optical efficiency Two issues are raised by exotic modes. The first one is: since the usual lasers oscillate as TEM_{00} , how to generate such modes? The second is: what are the new requirements for the angular control system, since stronger interaction with mirror misalignments are expected?

Mode generation Exotic modes have been also proposed in a different context. Power laser builders are also confronted with spurious thermal issues and undesired non-linear effects in general, and had the same reflex of spreading the power. Special solutions have been developed starting from a conventional TEM_{00} laser, then coupling the light into a high order LP (linearly polarized) mode of an optical fiber through a grating. Some LP modes have structures analogous to LG modes (fig. 21). At least 75% of the power of a laser could be coupled in the desired LG mode after very preliminary calculations. Theoretical studies are in progress to determine the maximum of coupling. Experimental studies are planned for checking the results.

Mirror displacements and consequences The effect of small rotations and displacements of the mirrors has been studied using the DarkF code by M.Laval. For summarizing, the HOLM are rather sensitive to transversal displacements, and the Mexican modes to rotations.

Conclusion and perspectives From a theoretical point of view, HOLM are extremely appealing. They seem to cure at the same time thermal noise and thermal issues. Especially using LG modes seems to be promising, since no special shaped optics are required. Experiments are needed (and planned) to actually produce such modes. Simulation is still necessary (and planned) to give realistic requirements on the control system.

10 Interferometer sensing and control

10.1 Length sensing and control

The longitudinal sensing and control in AdV must deal with the control of five degrees of freedom. Four of them are the same already controlled for Virgo and Virgo+ (the differential and common combinations of the arm lengths, the length of the power recycling cavity and the short Michelson). The additional degree of freedom is given by the length of the signal recycling cavity.

The development of a control strategy for AdV can be split in two main conceptual works. It is first necessary to study the response of different optical signals to all the five degrees of freedom, to understand which signals might be used for the control in the steady state configuration. This implies the evaluation of several points:

- how many optical signals are needed, or in other words if there is the necessity of having pick-off beams in addition to the standard ones;
- which and how many modulation frequencies are needed;
- which is the best control strategy for the signal recycling control, in particular understanding the amount of coupling of this degree of freedom (dof) with the other ones;
- moreover, the signal recycling control loop should allow the possibility of tuning its working point;
- the requirements on the locking accuracy (the residual RMS fluctuations of the controlled degrees of freedom) has to be computed and compared with the expected actuation performances;
- the actuation dynamical range required to maintain the system locked must also be evaluated.

The second part of the work involves a deep study of the lock acquisition strategy, meaning the sequence of actions that brings the interferometer from a completely uncontrolled configuration to the final state. The actual lock acquisition strategy (based on the Variable Finesse technique) must be revised and possibly adapted to the new optical configuration. It might turn out that a completely new strategy has to be developed. This also includes the evaluation of the needed actuators dynamical range to acquire the lock. Non-linear reconstruction techniques might be needed to compute the mirrors motions and bring the system on resonance using low forces.

So far only preliminary simulations have been performed. These effort should continue with the development of ad-hoc simulations both using time-domain tools (like Siesta) and frequency-domain tools (like Finesse). The development of the control strategy and maybe of the lock acquisition technique can benefit from the work already carried out inside the LIGO collaboration. Moreover it will be possible to test the lock acquisition with table top and suspended experiments at CALVA.

10.1.1 Status of the related R&D (CALVA)

The CALVA purpose is to investigate a new lock acquisition scheme involving auxiliary lasers. Briefly, the main idea is to control each degree of freedom with a dedicated laser independently from the other dofs. Once each dof is under control, the interferometer is brought in a deterministic way to its working point where the linear locking can be activated. It should be underlined that this technique will have no effect on the sensitivity of the instrument but we think that it will speed up the commissioning of the instrument. The aim is to be close enough to AdV parameters in order to validate the major technical choices made for the locking and alignment loops. Thus, the down-time for the transition from Virgo+ to AdV will be minimized and we can hope to bring AdV to its nominal sensitivity as fast as possible. This is the primary goal of this facility. According to the planning for AdV and for this facility, it can be foreseen to implement ideas which have lower priorities for the moment: use of flat beams, squeezing or all-reflective optics or to increase the complexity of the optical layout in order to be closer and closer to the AdV one. A lock acquisition technique using auxiliary lasers which will be used to freeze the cavities lengths will be investigated. The auxiliary lasers have a different wavelength compared to the main one. So, they will see a less reflective coating leading to lower finesse and less coupled cavities. The lock acquisition of such cavities will be easy. Once the cavities are locked using auxiliary lasers, their working point will be slowly shifted introducing an offset in the control loops (which use error signals generated by the auxiliary lasers) and/or changing the auxiliary laser frequency in order to bring the main laser to resonance. Then, a smooth transition will be performed in order to use error signals generated by the main laser. If this scheme is successful, it could be used as guidance for the lock of any complex optical configurations. If the quality of the alignment is an issue (this point has to be investigated), one can envisage to use the auxiliary lasers to perform a pre-alignment sufficient to perform the locking with the main laser. The Virgo commissioning has clearly shown that the lock acquisition can be very sensitive to alignment conditions.

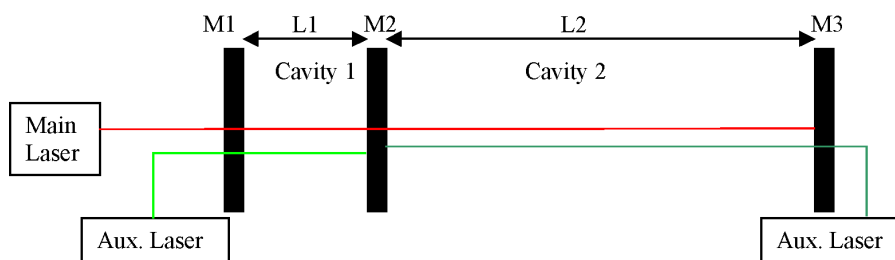


Figure 22: Optical configuration of the test facility. For clarity, the various beams have been vertically shifted. In real conditions, they should overlap in order to see the same cavity length.

The challenge for CALVA is the locking and the alignment of two coupled cavities illuminated by a high power laser (see Figure 22). The first cavity is a low finesse and short cavity while the second one is a high finesse and long cavity in order to mimic the behavior

of the power/signal recycling cavities versus Fabry-Perot cavities in AdV. It should be underlined that two coupled cavities can be locked using only one auxiliary laser but this scheme can not be easily extended to more complex configurations like the AdV one where at least four and probably five degrees of freedom are coupled. So, it seems reasonable to investigate a system where all cavities are treated in an independent way. Once the lock will be acquired in a repeatable and robust way, the effects of the radiation pressure on the cavity stability will be investigated. In particular, the coupling with angular degrees of freedom will be investigated and an automatic alignment will be implemented. The main outcome of this scheme is a more robust and simpler lock acquisition scheme and we hope that it can speed up the commissioning of AdV. It can also lead to a reduction of the maximal forces applied to the mirrors and thus it can help to relax the constraints on the actuators for AdV. A two phases installation has been planned in order to share the cost over the years. In the first phase (2008), only the short cavity but with a high finesse will be installed, to test the technique in the simplest conditions. Then, in the second phase (2009), the two coupled cavities will be completed. A detailed planning is available in [46]. At the moment the hall which will house the experiment is not yet available due to works for asbestos removal. This will delay the start of the installation by a few months. The design of the mirror tank is finished and the group is ready to send the call for tender. The design of the suspension is almost finished and some pieces are already in production. A first version will be available in December. The design of the optical benches has been started.

10.2 Alignment sensing and control

The alignment system consists of several systems which use control systems to align the core optics during the various modes of operation of the interferometer. In the following we concentrate on the continuous global alignment control which would provide the low-noise alignment control during science mode.

The alignment system designed for the Virgo detector, based on a unique RF modulation-demodulation scheme, cannot be used directly for AdV. First of all the introduction of the signal recycling mirror will add a new level of complexity for the resonance conditions of the RF sidebands. No dedicated R+D has been started yet, but the commissioning experience of the Virgo interferometer indicates that the following issues have to be investigated:

Pick off beams for alignment control: The main difference for the alignment control between the Virgo and the AdV configuration is the presence of the Signal Recycling mirrors which, except from the increase on the complexity of the RF sidebands, adds degrees of freedom to be controlled. Thus in total we should control the four cavity mirrors, the BS mirror, the Power Recycling mirror (PRM) and the Signal Recycling mirror (SRM). This requires an equal amount of independent optical control signals. It is not obvious how many beams leaving the interferometer are required to generate the required signals. It might be necessary to use all possible beams, including so-called

pick-off beams generated at the AR coating of the core optics. The use of pick-off beams requires wedges in the core optics substrates (see Section 9.3). Further the optical layout has to accommodate for the extra beam, both inside the vacuum system and in the readout systems on the optical benches outside the vacuum.

Use the signal in transmission: In order to reduce the control noise the sensors used for generating alignment control systems must be shot-noise limited while detecting a large enough fraction of the outgoing beams. A simple method for generating suitable beams would be to use the light transmitted by the arm cavities. For using these beams, an alignment control scheme based on mixture of Ward-like and Anderson-like RF sidebands could be developed, i.e. at least one modulation frequency is tuned to have the first higher transversal mode of the upper sideband resonant into the long arm cavity, in order to have enough power for the signals in transmission. In addition at least one modulation frequency not resonant in the arm cavities (in any mode) is used to generate high power pick-off beams in the central interferometer.

The use of the pure Anderson-Giordano technique: As it has been shown during the development of the alignment control system for the Virgo interferometer, the *Anderson-Giordano technique* in its pure form could not be applied, due to the fact that one degree of freedom was only poorly controlled. In fact to control this dof, the common mode for the end mirrors, an additional readout using a modulation frequency which is not resonating into the recycling had to be implemented. Thus for the AdV, which features an additional dof with respect to the Virgo interferometer, the original Anderson-Giordano technique can definitely not be used.

The side-effects of using the same modulation frequency for the angular and longitudinal control: The main effect of using the same modulation frequency for both control system is a more direct coupling between the two control systems. In fact, during the Virgo commissioning the coupling between the longitudinal and the angular signals was a limiting factor, especially at low frequencies (below $\sim 100\text{Hz}$), in the reduction of the control noise. Moreover the use of a RF sideband resonating as a TEM_{01} mode in the arm cavities caused alignment depended offsets in the for longitudinal error signals.

Parametric instabilities: According to the research by the LSC groups the higher circulating light power in the arm cavities might give rise to parametric instabilities. We have not yet evaluate the order of magnitude of the effect of these instabilities in possible optical layouts for AdV. A dedicated R+D programme should be initiated. In addition, even in an optimised optical layout will make a control system design more difficult as the traditionally used control matrices and simple optical transfer functions will not be enough to describe the interferometer.

Advanced Virgo Conceptual Design:

PART 2:

Test mass vibration isolation, suspension
and control

11 Superattenuators

The isolation performance of the Virgo Superattenuator (SA) is expected to be compliant with the requirements of AdV. Therefore, no major changes to the vibration isolation system are required. However, the experience of the Virgo commissioning has shown that some aspects of the design can be improved:

- the Virgo inverted pendulum (IP) is controlled in 4 d.o.f. only (the three translations and the rotation around the vertical axis). It has been understood that the ground tilt, especially in windy days, spoils the performance of the inertial damping and causes low frequency noise to be transmitted to the mirror. Therefore, the SA design has to be modified to allow tilt control;
- the design of the SA bottom part is very complicated. A new one has been proposed, using a recoil mass for the marionette, that would simplify greatly the procedure for the suspension of the payload, reduce the mirror contamination during this phase and allow the implementation of a clean air flux in the bottom part of the tower;
- a new reference mass (RM), compliant with the thicker mirrors and with the requirements of the thermal compensation system must be designed. The design will be different whether electrostatic or electromagnetic actuators are chosen;
- the marionette will suspend a monolithic payload.

11.1 IP modifications and tilt control

The present VIRGO pre-isolation stage, the IP, must be upgraded to be controllable in all six d.o.f., using tiltmeters as sensors for the rotational d.o.f. (see sec. 11.2). Since the beginning the mechanical structure of the IP was designed taking into account the possibility to implement a tilt control: an elastic element was embedded within its feet (see fig. 23) and the space for inserting PZT actuators was foreseen. Each IP leg can be thus acted upon in the vertical direction to compensate the tilt effect measured on the IP top stage. In this way, the IP top stage could become an inertial platform controlled in 6 d.o.f.. Moreover, a complete revision of the leg structure, changing it in a monolithic one with an increased sectional area (higher momentum of inertia) will move at higher frequency the annoying leg resonance now at about 10 Hz.

Also the low resonance mode of the Filter Zero (F0) crossbar falls in the same region. Such structures in the IP transfer function reduce the attenuation performance and make difficult to widen the control bandwidth of the inertial damping. Therefore, it would be helpful to revise the F0 design making the crossbar more rigid. A simple way to do that could be the removal of the two vertical accelerometers accommodated on it. An alternative or complementary solution could be the development of a more compact hoist mechanism for the wide vertical motion of the suspension point (± 35 mm) to be accommodated within the crossbar structure. Even in this case the reduction of the total weight pushing on the crossbar structure could be relevant for the final goal. As a

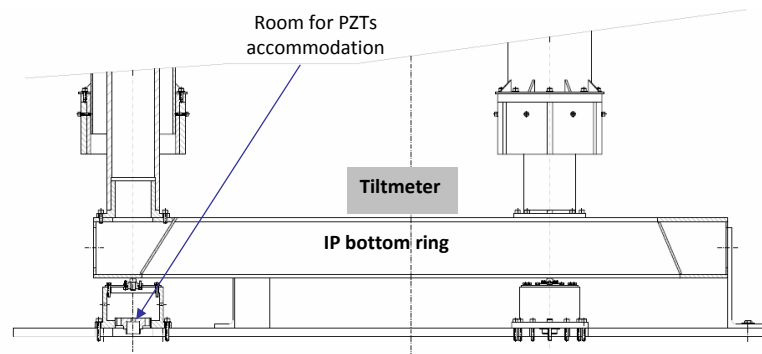


Figure 23: The IP bottom part is visible. A section of a foot supporting the IP bottom ring and the last part of IP leg is visible on left side. A schematic box representing the tilt meter accommodation is also shown.

consequence of this intervention an alternative design for the vertical damping should be studied.

11.1.1 Status of the related R&D

The INFN Pisa group is involved in the design, development and construction of a new mechanical structure of the IP. Starting from the present design and reducing the impact of the changes at the minimum level a new IP design has been developed (see fig. 24). Monolithic legs (about 6 m tall for the long SA) and increased sectional area will move the leg resonance at higher frequency.

11.2 Tiltmeters

The operation of Virgo has shown that the inertial damping performance is partly spoiled in presence of strong wind. This has been explained as an effect of wind-induced ground tilt. The tilt messes up the signal of the in-loop horizontal accelerometers and this turns into low frequency noise transmitted to the mirrors. This makes the VIRGO lock acquisition more difficult with bad weather conditions and the effect will become even more relevant in AdV. An active control of tilt should then be implemented to make the detector more robust. It requires the development of an angular sensor with sensitivity around 10^{-8} rad/ $\sqrt{\text{Hz}}$ at 10 mHz [47]. The activity in progress is focused on the study and the development of tiltmeter based on a device conceived around a pivoted bar with an LVDT sensor (see fig. 25). This sensor will be installed within the vacuum vessel of each SA on top of the bottom ring (see fig. 23) supporting the inverted pendulum legs where room is available.

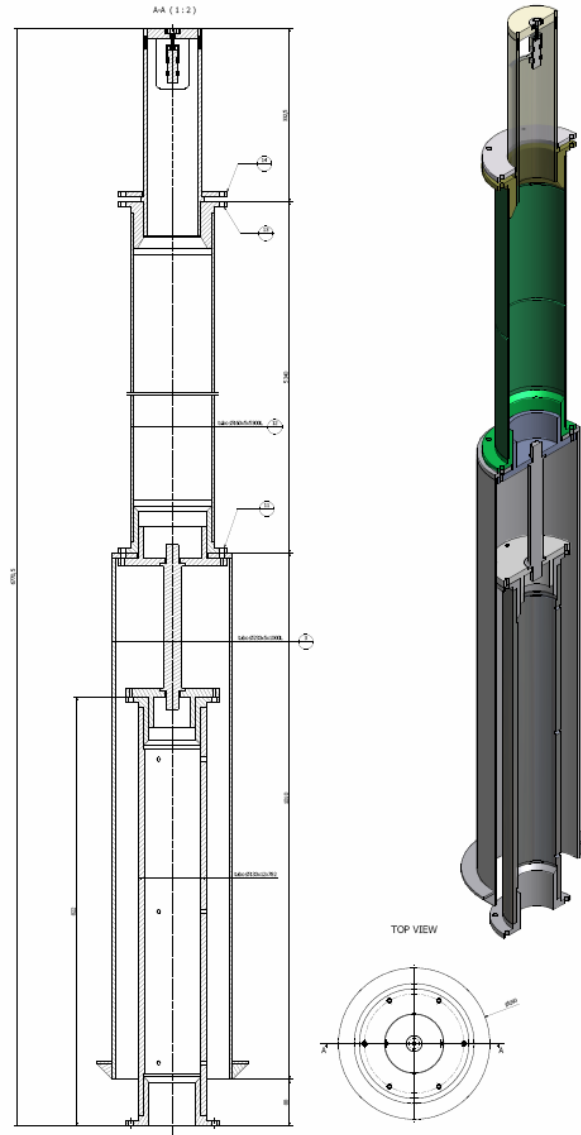


Figure 24: Technical drawing of the new IP based on monolithic legs with increased sectional area. The visible length of the leg (green) is not in scale.

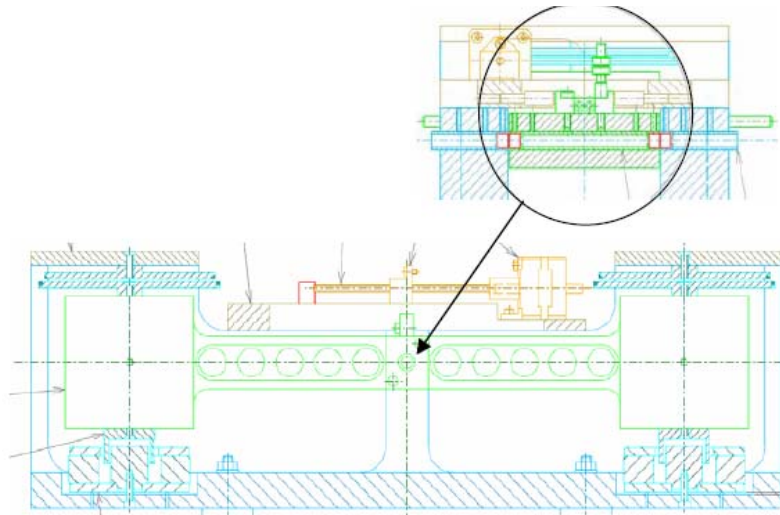


Figure 25: Technical drawing of the tilt meter prototype. Within the circle a detail of the device pivoted bar is shown.

11.2.1 Status of the related R&D

Two groups are involved in this activity: INFN Pisa and INFN Roma Tor Vergata. Two identical prototypes have been machined and they are under test at INFN Roma Tor Vergata laboratory.

11.3 SR SA

A complete long SA must be assembled to suspend the SR mirror. It will be provided with all the upgraded parts (new IP legs, tilt control, new payload).

11.4 Short SA upgrade

During the Virgo commissioning activity there have been several hints that the seismic isolation provided by the short suspensions (IB and MC) could be not enough. We propose to add one seismic filter to the short SAs suspending the injection bench, the IMC end mirror and the detection bench. This will allow to improve the isolation performance and is an easy operation.

Tilt control will also be implemented on the short towers, while IP legs will not be changed, since they are already monolithic.

11.5 Suspensions Last Stage: marionette reference mass

A new configuration for the last stage suspension system is being studied for AdV. It will include a new element: the reference mass of the marionette (MRM). The new design is conceived having in mind two main objectives:

- to guarantee a high level of mirror cleanliness without spoiling mechanical performance of the suspension system;
- to simplify the payload installation and its preliminary alignment procedure.

The vacuum chambers hosting the superattenuators (about 10 m tall) have a volume of about 30 cubic meters and are divided in two sections: the upper part hosting the IP and the chain of filtes, and a lower part where the marionette, reference mass and mirror are hung. The two sections are divided by a separating roof (see fig. 26) consisting of two metallic plates (about 2 m in diameter) forming an Intermediate Vacuum Chamber (IVC). This technical solution allows the two compartments to be kept at different vacuum level: 10^{-6} mbar of total pressure for the tower upper part and 10^{-9} mbar for the UHV chamber where the mirrors are accommodated. Moreover, the IVC structure represents a very good mechanical protection from any contaminant and pollution of the mirror environment.

The separating roof structure is completed with four pots bolted on the second plate. These pots are adopted to enclose, in the low vacuum level (10^{-6} mbar) volume, the legs of the Filter 7 (F7) and the coils acting on the marionette magnets. The two vacuum compartments are in connection only through a conductance pipe used as a passage of the suspension wire connecting the payload to the F7 (see fig. 27).

In order to simplify the assembly procedure and to reduce the human presence in the vacuum chamber in that phase it is necessary to review the last stage structure and its interface connection with the F7. Changes in the suspension system structure will also have an impact on the hierarchical control strategy of the mirror. A structural change of payload and F7 will require to study the new dynamic behavior, a new mode identification and a careful compensation of the recoil effect. The MRM will be installed, as an additional suspended element, within the UHV chamber between F7 and marionette replacing the F7 legs. It will host the actuator coils for steering the marionette. In this way a more compact design of the payload will be conceived and the IVC structure could be revised to accommodate a mechanical filtering system for the air flow entering within the UHV chamber. Following these project guidelines, the payload integration on the suspension system will benefit of:

- a wider clearance for the monolithic payload assembly, reducing the permanence time of two operators within the high vacuum chamber for its final installation;
- a quasi-laminar flow of clean air within the UHV chamber volume to be used during the assembly phase (TBC).

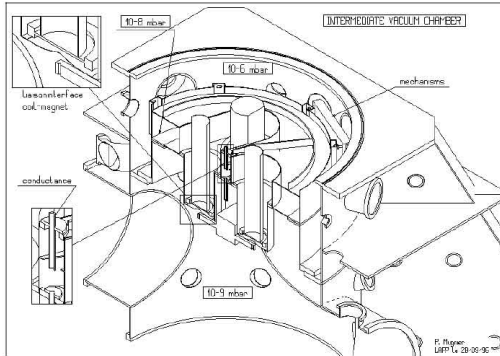


Figure 26: Sectional view of the base tower with the Intermediate Vacuum Chamber, the pots and the conductance pipe.

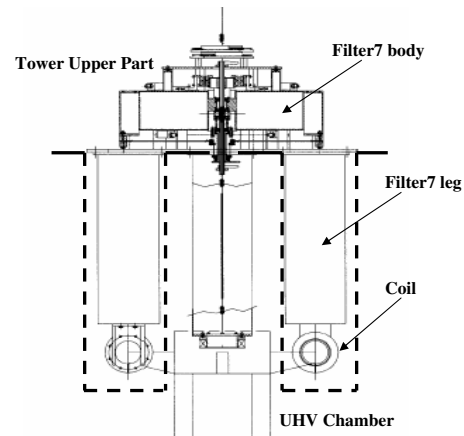


Figure 27: Technical drawing of the F7 body and legs. The dotted line in the picture represents the separation limit between the two vacuum compartments obtained bolting the pots on the second plate of IVC. The mechanical support (F7 legs) of the coil actuators faced to the marionette permanent magnets is also visible.

11.5.1 Status of the related R&D

The activity is performed at INFN Roma1 laboratory in collaboration with INFN Pisa personnel. A preliminary design has been developed for a MRM prototype in reduced scale. The assembly procedure of this prototype proved it to be not as good as expected from the payload handling point of view (some difficulties have been found in assembling the coil-magnets pairs and other mechanical elements). A second design, based on a different geometry, is in progress. A check of this new version will be done with a finite element analysis.

11.6 Suspensions Last Stage: New marionette

The SA last stage must be redesigned in order to include the MRM. To this aim the other components must be reviewed also because the new mirrors have larger mass and different thickness and must be suspended with silica fibers. Moreover the whole payload must be compatible in shape and materials with the thermal compensation system (see sec. 7).

The new marionette is designed to allow the fibers to be welded on the silica clamp which must be hosted in a suitable support. The connection of the fiber to the clamp must be lossless and is designed in such a way to avoid any risks of fiber rupture, both during

the assembly and welding procedure and during the operation. The usual requirements for cleanliness, vacuum compatibility, mechanical precision and magnetic and electrical properties apply. The clamping point, as in the Virgo payload design, must lay on the horizontal plane passing through the center of mass of the marionette, to minimize the coupling between different degrees of freedom. This requirement is more difficult to meet for a monolithic suspension because usually in this case the clamping section does not coincide with the bending section. A study of this aspect is needed. The design of the coupling between marionetta and fiber will also influence the assembly procedure of the payload and must be finalized when the full mounting sequence will be established. Finally, the new design will require a revision of the clamping setup for the reference mass, and eventually of the balancing motor. A complete FEM analysis of the new marionetta, together with a measurement of resonance modes will be performed.

11.7 Suspensions Last Stage: new reference mass

The new RM design will take into account the requirements related to the heavier mirrors, improved mirror control and thermal compensation system. The overall characteristics of current RM are kept. The RM surrounds the mirror in order to protect it by the dust coming from the top and it hosts the actuators for the mirror control purposes. The RM center of mass must coincide with the mirror one. This is a crucial point for the positioning and control system because it prevents the couplings between torsional and translational degrees of freedom. The actuators have to be dimensioned to fulfill the displacement requirements for the locking purposes and consequently are related to the optical configuration. Moreover these actuators must not introduce extra noise that can spoil the sensitivity curve.

As far as the actuators are concerned, there are two different options.

Coil-magnet actuators If coil-magnet actuators are used [48], the RM must be made of a dielectric material in order to avoid eddy current dissipation and magnetization effects. The mechanical strength of the new insulating material must allow to use the reaction mass also as a safety structure for the mirror. The design of the RM can be similar to the one of Virgo+ which is composed by different parts: an inner dielectric hollow cilinder which holds the coils and is in direct contact with the mirror sides and an outer stainless steel part, far from the coils, which makes the RM structure stiffer and increases the overall mass. The dielectric material must be chosen to be UHV and white room class 100 compatible. The use of a dielectric material could give rise to the problem of the mirror static electric charging by friction with RM. A solution can be the use of dielectric materials having a finite high resistivity that avoids the formation of stray currents but reduces the presence of static charges. The market offers several kinds of high technology plastic or ceramic materials that can be useful for our purpose. A possible choice is the TecaPeek CF30, a kind of polymeric plastic, loaded by carbon and grafite particles so that to increase its density and to have a slight electrical conductivity which is useful to avoid the static charges formation. This material will be used for the Virgo+ update and it is

being tested in this frame. For an advanced configuration other hi-tech materials will be studied in order to improve the performance of the system.

Electrostatic actuators In this case the use a dielectric material is not needed anymore, but the electrostatic charging can be present anyway because of the nature of these actuators. The problem can be partly solved by using an AC polarization of the actuators (see sec. 11.8). All the material must be UHV compatible and white room class 100 compatible. The new RM must be shaped in order to host the new thicker mirror (20 cm instead of 10 cm of Virgo). The RM is also equipped with safety stops that will have to be redesigned taking into account the different shape, the increased mirror masses suspended with a monolithic structures. The aim is to realize soft stops made of electrical conductive material in order to avoid the mirror charging.

The RM design must be compatible with the thermal compensation which foresees to install ring heaters suspended from the last stage of the SA or embedded into the RM itself, and the use of a compensation plate anchored to it. To this aim, all the material of the RM must work in presence of the heaters and a study of the dynamical and thermal behavior of the overall suspension system must be performed. In particular the presence of a compensation plate could deeply affect not only the RM design but also the dynamical behavior of the last stage suspension system. This aspect must be carefully studied and a very close interaction between the two groups must be considered.

11.8 Suspensions Last Stage: electrostatic actuators option

An interesting alternative option for the control of the suspended mirrors is the use of electrostatic actuators (EA). This solution, already proposed years ago [49], was implemented on GEO600 [50] with good performances, and other research groups are currently working on it for the implementation on Advanced LIGO. The full characterization of a typical EA can be found in [51].

The use of EA could offer several advantages with respect to the coil-magnet one. The first evidence is the possibility to use the mirrors as they are, without the necessity to glue the magnets on them. This give, of course, an immediate benefit in term of reduced contamination of the mirror surfaces during the preparation of the payload. But the main advantage is the reduced degradation of the mechanical quality factor of the test mass [52]. Another advantage is the strongly reduced coupling with external magnetic fields. A residual coupling could arise at the level of the marionetta, that is still controlled by magnet-coil pairs, but in this case the residual noise requirements are more relaxed. On the other hand, any possible coupling with variations of external electric fields, is largely reduced thanks to the high electrical conductivity of the vacuum tank.

On the other hand, also some drawbacks are expected. The most important are summarized in the following. A reduction of the quality factor both for the suspension as well as for the test mass itself is foreseen, as reported for example in [53] [54] [55]. This damping effect seems also related to the geometry of the system and to some working condition, as,

for example, the frequency of the actuation signal or the electric field intensity. Another problem arises since the EA can only pull the test mass respect to the actuator, as a consequence, in order to achieve an effective displacement control of the mirror it is necessary to use a bias voltage. This can generate two different problems. The first one is related to the presence of stray electrical charges on the dielectric test mass, that can couple with the strong electric field generated by the actuator resulting in an increasing force between the mass and the actuator that produce a slow drift as final effect. The second one concerns the improved actuation noise due to the this large bias. Another possible source of noise can be the joule dissipation inside the actuator electrodes, in particular if the driving voltage is at high frequency. The heat dissipation can result in extra thermal noise for the mirror. Finally the distance between the actuator and the test mass has to be fixed taking into account the safety conditions for the monolithic suspension that will be adopted in AdV.

The aim of the R&D program is to evaluate if this kind of actuation system can be effectively used in AdV, replacing the existing coil-driver system.

11.8.1 Status of the Related R&D

The main topics to investigate in the R&D program are shortly described in the following:

- Design of the EA pattern: this is a very important point, in fact there are several characteristics directly affected by the pattern used in the actuator design. A first one is the maximum force achievable for a given polarization voltage applied on the actuator. A model of the characteristics of a simple geometry actuator [51] can be used as a starting point for the pattern design. Of course a better calibration is needed directly on the actuator implemented on the reference mass. The parameters to optimize are the distance between the mirror and the actuator and the distance between each electrode of the actuator. Also the thickness of the electrodes should be optimized in order to minimize the power dissipation that can generate thermal noise. Finally a careful design study of the reference mass, with the EA directly integrated in its internal surface, is needed to minimize the effect of misalignment between the actuator and the test mass.
- Study of the actuator driving technique: a suitable high voltage amplifier has to be used in order to polarize the electrodes of the actuator. A simple DC amplifier represents the easiest solution. Since the forces obtained by such actuators are always attractive, a DC bias is needed to effectively implement the control. Moreover a study of an AC driving performances is needed to reduce the noise arising from stray charges on the test mass [56]. In this last case, further noise can arise from the coupling of patch charges on the mirrors with the electrode's pattern.
- Reduction of coupling noises: even if no direct coupling with external magnetic fields is expected, it is important to evaluate the coupling with external electric fields and charges. For the same reason the design of the EA has to be performed in order to minimize the residual electrical dipole. Moreover, since the actuator is

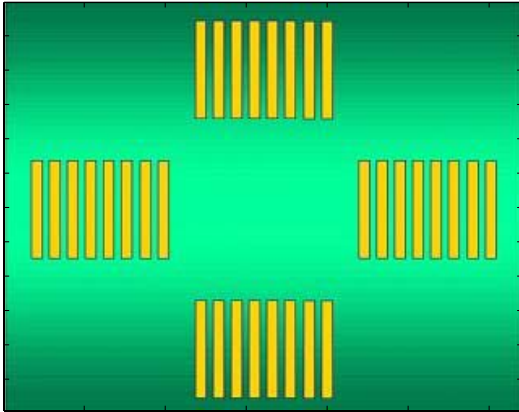


Figure 28: Layout of the initial actuator

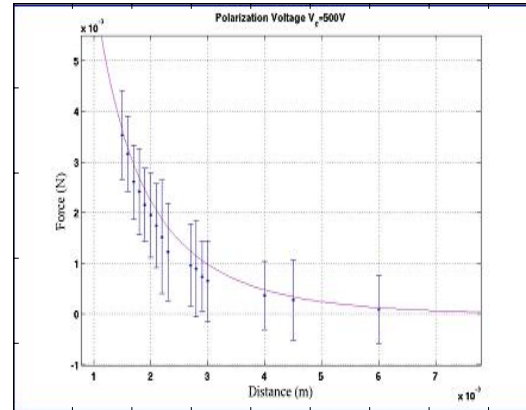


Figure 29: Force vs. distance: model and measurements at 0.5 kV

composed by, at least, four sub-actuators, a careful study of the cross-coupling has to be carried out, to reduce unwanted effects during the control. Finally, since the AC driving cannot mitigate the effect of a dynamical charging of the test mass, it is important to evaluate (with the help of a suitable simulation tool) and to measure the noise induced by this effect.

- Study of the limitations due to the quality factor reduction expected for the presence of the strong electrical field. In particular it is necessary to verify that the foreseen quality loss is compatible with the requirements fixed for the AdV noise budget

Some steps of the R&D program were already fulfilled, and the first results are reported in the following.

The action of an EA, composed by a simple array of electrodes polarized at opposite voltage is fully discussed in [51] by using a model based on the image charge. In the first step of this R&D activity, that simple model was slightly improved to take into account higher order terms in the expression of the force between the actuator and the dielectric mass. Only a small difference with respect to the old model arise from the new one, even if such difference increases as the distance between the actuator and the test mass decreases. On the basis of the model, and assuming a distance between the actuator and the mirror of about 1 mm, a simple 4-patterns actuator was designed and characterized (figure 28). The length of each electrode is $a = 4$ mm, the distance between each electrode is $b = 5$ mm, the height of the electrodes is $L = 4$ cm and the number of electrodes for each pattern is $N = 8$. The test mass used in this phase was a plexiglass cylinder with a diameter $d = 14$ cm and length $l = 10$ cm. As readout system, a standard optical lever was used to measure the position of the test mass.

The distance between the electrodes was chosen in order to allow a polarization as high as 2 kV, without perforating the dielectric substrates. The other dimensions, as well as the number of electrodes, derive from the space available to actuate on the test mass and from the theoretical model. This actuator was characterized using a suspended dielectric mass

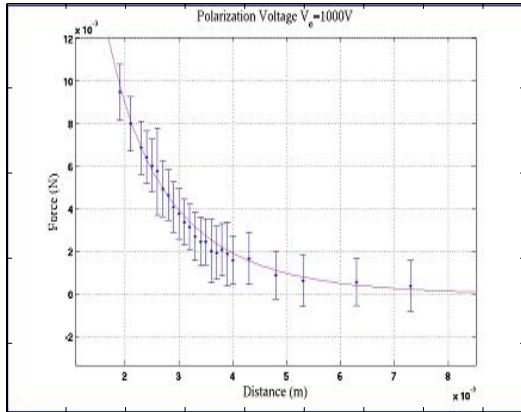


Figure 30: Force vs. distance: model and measurements at 1.0 kV

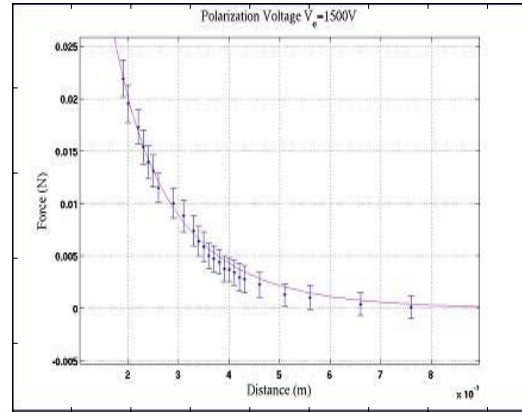


Figure 31: Force vs. distance: model and measurements at 1.5 kV

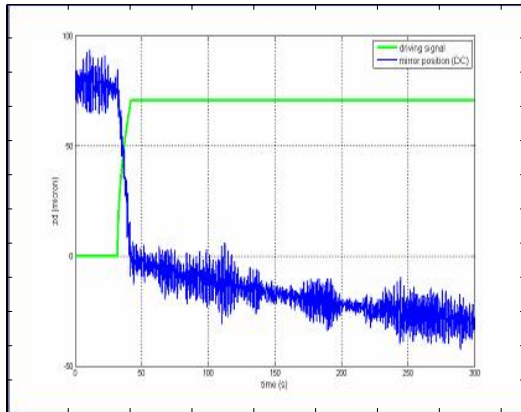


Figure 32: Position drift in DC driving.

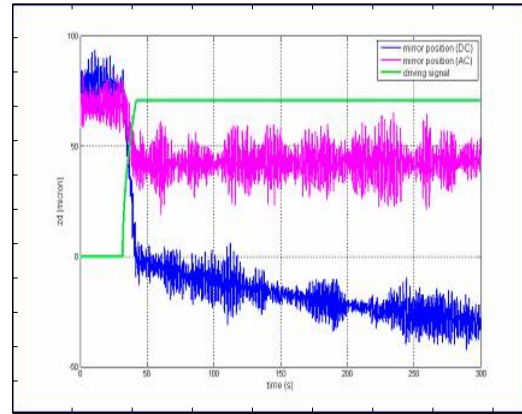


Figure 33: Comparison between AC and DC driving.

whose position is read by an optical lever. Several measurements of the displacement of the mass, as a function of the actuator polarization and of the distance between the actuator and the mirror were performed giving good agreement with the model (figures 29,30,31).

Another feature of the actuator is the influence of the electric charges that can be found on the test mass. Since the actuator generates also a static electric field, it is clear that any unbalanced charge on the test mass produce an additional force on the mass itself. This effect is very well visible on the prototype. As a driving signal is applied on the actuator, a slow drift of the test mass position takes place (figure 32).

The force acting on the mass can be expressed by:

$$F = \frac{1}{2} \frac{dC}{dx} V^2 + QE \quad (11)$$

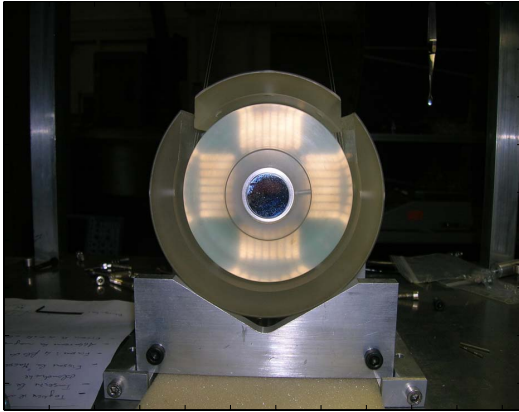


Figure 34: Suspended mass and electrostatic actuators.

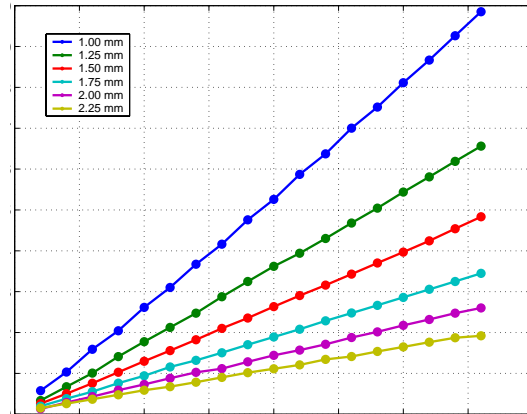


Figure 35: Force induced by the EA vs applied voltage for different distances respect to the test mass

where E is the electric field in the gap between the actuator and the mass, C is the capacitance and Q the net charge of the test mass. The second term of the equation (11) can be easily reduced by using an AC driving. This can be done by modulating the correction signal at high frequency. In this way the residual electric field has no static component and the net electric charge do not produce any drift. Moreover, the first term of the (11) remains almost unchanged, since it depends on the square of the voltage. In fig. 33 the effect of an AC driving is reported. It is clear that no appreciable drift was induced by the driving. In the measurement the actuation signal was a simple sinusoidal voltage with a frequency $f = 500$ Hz. Moreover, since it is better to work in terms of forces, in particular in view of the control system development, the signal sent to the actuator is the square root of the control signal, as a consequence of the quadratic term in (11).

The generation of the sinusoidal bias and the square root operation are performed digitally. This choice put a limit in the maximum frequency achievable for the AC bias in the prototype, since the maximum sampling frequency of the control and data acquisition system system is currently fixed at 5 kHz.

In parallel to the test activity, a new kind of actuator was designed and realized. It will be used on the reference mass of a suspended mirror. Its size is smaller respect to the size of the prototype, since the new test mass has a reduced size. Also this actuator has 4 symmetric patterns in order to actuate in the same degrees of freedom of the prototype. Of course both the reference mass and the test mass are dielectric to avoid charge motion close to the test mass. The new actuator has $a = 4$ mm, $b = 5$ mm, $N = 8$ and $L = 2.5$ cm, while the test mass, also in plexiglass, has a diameter $d = 10$ cm and length $l = 6$ cm. The suspended test mass and the new actuator fixed in the recoil mass of the suspension are shown in figure 34.

This new actuator was first characterized by taking the recoil mass fixed respect to the ground. To avoid any effects due to the stray charge drift the measurements were performed only in AC driving condition. In particular the displacement of the test mass was measured for different distance and applied voltage, but with a fixed frequency of 200 Hz. The result are reported in fig. 35. A very good linearity with the square of the voltage is evident.

Of course, other measurements are needed to completely characterize the actuator. For example it is important to understand the behavior of the force F as a function of the frequency of the AC bias.

Moreover a detailed study of the quality factor degradation is required, even if old and recent works in this field already give some indication. For this kind of measurements the experimental set-up will be placed in a vacuum tank, and, of course, the initial test mass will be replaced by a fused silica cylinder. In the first phase of this R&D step, the standard actuator designed on a vetronite substrate was used, but in the second step of this study it is necessary to move toward a more realistic set-up. In particular, since the choice for the future recoil mass of AdV, is a dielectric, vacuum grade, substrate (the tecapeek is the most promising), it will be necessary to realize an actuator on the same substrate. In this case the pattern has to be realized by metallic evaporation or sputtering as well, depending on the property of the substrate. Moreover a full scale prototype has to be used in this step, in order to perform a realistic evaluation of the system performances.

Finally a careful study will be devoted to the design of the driving electronics, as well as to the wiring of the actuator. Up to now, in fact, a commercial high voltage amplifier was used, one for each pattern of the actuator, while the AC bias was digitally performed. For the future it will be better to have a suitable home-made electronics, both for the lower cost and for the more appropriate design. Moreover an analog oscillator should be used to produce the AC bias, in this way it will be possible to increase the frequency of the bias, in order to not introduce any interference in the measurement frequency band.

12 Monolithic suspensions

This project is devoted to the realization of a monolithic fused silica (FS) suspension for the four Fabry-Perot cavity mirrors heavier than the respective ones in Virgo. The main aim is to study the optimal geometry and technology for the mirror suspensions with the objectives of i) minimizing the thermal noise of the centre of mass, ii) fulfill the requirements for an optimal control of the suspended mass, iii) guarantee safety and reliability. At the moment the monolithic suspensions have been realized attaching silica fibers to the mirror by welding them to intermediate components (called ears) silicate bonded to the lateral flats of the mirror itself. Although this solution has been successfully implemented in GEO600 the silicate bonding technology remains the most critical item of the whole system for two main reasons: i) at present there is not any non-destructive test to perform on the bonding, apart the visual inspection; ii) the replacement of an ear or the bonding of a new ear on the same surface where an old one has been attached may put in serious risk the quality of the mirror coating. For these reasons an investigation to develop another technology able to replace silicate bonding is regarded as relevant and in time with the R&D program for AdV. The solution suggested in this proposal consists of machining the ears out of the test mass lateral surface. Although the idea is not new, in the present proposal an R&D plan to overcome the difficulties specific of this solution is shown. More details can be read in section [12.3](#).

12.1 Geometry and dimensions

In this section the preliminary considerations that drive the design of the monolithic suspensions are presented. Breaking strength is not the only parameter that matters.

12.1.1 Mirror geometry

The mirror geometry is the first set of parameters to fix and it is independent from the type of suspension chosen. Large mirrors are to prefer because the laser spot can increase to the benefit of the coating and substrate thermal noise. Moreover, the total mirror thermal noise is a reference for the suspension thermal noise: the noise level of the suspension has to intercept the mirror noise level below the frequency where other types of noise start to be dominant (seismic, Newtonian and control noise mainly). In this proposal a Suprasil 312 of about 40 kg mass (35 cm diameter, 20 cm thickness) has been assumed with an high reflective coating having the lower loss achievable today. It has to be noticed that the possibility to have a larger mass or a better aspect ratio has to be investigated.

12.1.2 Bouncing mode

Fibre length, fibre stiffness and position of bending points are driven by the room available and the choice of resonant frequency of the various modes of the suspension. This choice depends strongly on control issues and a careful investigation has to be carried out. At this moment fibre length and separation are maintained the same as in Virgo: 70 cm and 5 cm respectively. The vertical bouncing frequency of the last stage represents the lower limit of the detection band because although the vertical to horizontal coupling is small (it has been assumed 10^{-3}), the vertical oscillation does not have any dilution factor. The result is that the vertical bouncing mode is clearly visible in the thermal noise spectrum and in order to keep this frequency below 10 Hz the silica fibres have to work at an average stress higher than 380 MPa (80 kg is the assumed marionetta mass). For circular fibres it means an effective diameter smaller than 570 μm

12.1.3 Violin modes

In order to have the detection band with the smaller number of resonant modes as possible, the first violin mode should be as high as possible. The position of the violin mode depends on the fibre cross section and then ultimately on its breaking stress. Although fused silica fibres have a breaking stress in the range 2 to 4 GPa (lower values for larger diameters) the common practice suggest to do not load the fibres at stress higher than 800 Mpa. This value allows to have the first violin mode at about 430 Hz which is about 100 Hz higher than what can be obtained with steel wires. 800 Mpa of stress corresponds to a fibre diameter of about 400 μm .

12.1.4 Fiber shape

Due to the low thermal conductivity of silica the thermoelastic peak of 400 μm diameter fibre is at 11 Hz. At this frequency the fibres mode shape is almost straight and the only significant bending is at the upper and lower ends. Using the effect of non linear thermoelasticity it is possible to demonstrate that exists a stress at which the thermal expansion and thermal elastic compliance compensate each other and that this stress for fused silica is in the range 200 MPa to 250 MPa. All these data seem to indicate that the fused silica fibre with a dumbbell shape has the lowest thermal noise. A dedicated investigation on the optimal fibre shape will be carried out.

Suspension thermal noise using fibres of 400 μm diameter in the middle section and 800 μm at the two ends has been calculated and compared with suspension and mirror thermal noise in Virgo, mirror thermal noise in AdV and finally with the Newtonian noise. The results are plotted in figure 36 and they show that monolithic fused silica suspensions are required for the full exploitation of the new low loss coatings.

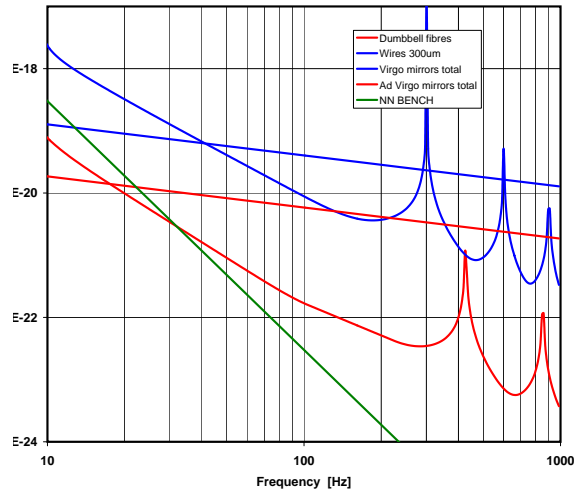


Figure 36: Comparison between suspension and mirror thermal noise in Virgo (blue lines), suspension and mirror thermal noise in AdV (red lines), Newtonian noise (green lines). The dumbbell fibres have a diameter of $800 \mu\text{m}$ at the ends and $400 \mu\text{m}$ in the middle section.

12.2 The ribbon option

The use of ribbons introduces another degree of freedom in the design of the monolithic suspension. The possibility to distribute the longitudinal load along the width of the ribbons maintaining a thin section and hence a very high dilution factor is indeed attractive. For a ribbon with aspect ratio of 10 the dilution factor increases of 10 times with respect a cylindrical fibre of the same cross section. The thermal noise spectrum goes with the square root of the dilution factor. The difference between ribbons and fibres is smaller at low frequency where the influence of thermal noise from upper stage becomes relevant. Moreover the vertical motion does not have any dilution factor and then there is no difference between fibres and ribbons around the vertical bouncing frequency. Finally, a significant effort has been spent in Glasgow to characterize the loss properties of ribbons that in principle may be different from the fibres one. In fact surface losses are dominant for such thin elements and preliminary results give to the ribbons an higher surface losses.

The sum of all these considerations can justify why ribbons does not have a large gain over the fibre as one could expect. On figure 37 the spectra of suspension thermal noise with ribbons and fibres are presented.

Although the production of ribbons is considerably harder than for circular fibres, the advantage of having suspension elements with larger cross section - and hence less risk - with the same noise performance is certainly relevant. The recent EGO R&D project granted to Glasgow goes in that direction and certainly it will contribute in a relevant way to the development of the Ribbons technology.

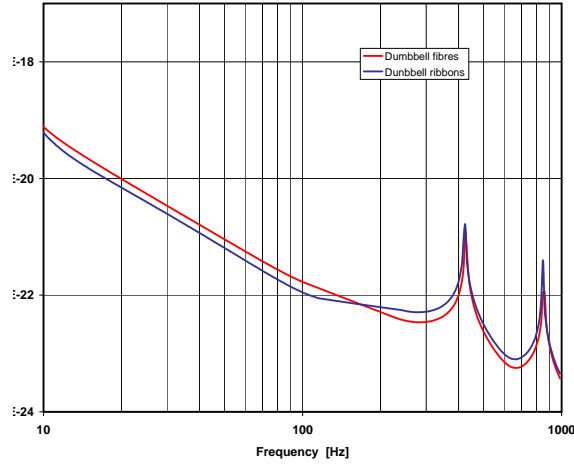


Figure 37: Spectra of suspension thermal noise of Ribbons as compared to Fibres. Both suspension elements have a dumbbell shape. As explained in the text several reasons, that have to be checked with a specific investigation, contribute to reduce the possible gain given by the ribbons.

M	40 kg	Mirror mass	C_{Sil}	$772 \frac{J}{kgK}$	Heat capacity of silica
L	0.7 m	Last stage pend. length	K_{Sil}	$1.38 \frac{W}{Km}$	Silica heat conductivity
d	$400 \mu m$	Fibre middle diameter	α_{Sil}	$0.51e - 6 \frac{1}{K}$	Silica th. expansion
D	$800 \mu m$	Fibre end diameter	β_{Sil}	$1.52e - 4 \frac{1}{K}$	Silica $\frac{1}{E} \frac{dE}{dT}$
t	$113 \mu m$	Ribbon middle thickness	E_{Sil}	$72.7 GPa$	Silica Young modulus
T	$226 \mu m$	Ribbon end thickness	ρ_{Sil}	$2200 \frac{kg}{m^3}$	Silica density
ϕ_f	$\frac{6e-11}{d}$	Fibre losses	σ_{Sil}	0.167	Silica Poisson ratio
ϕ_r	$\frac{1.5e-11}{t}$	Ribbon losses	ϕ_{Sub}	$1e - 9$	Mirror substrate losses
w_o	60 mm	Laser spot radius	t_{coat}	$2.2 \mu m$	Coating total thickness
n_{Sil}	1.4523	Silica refraction index	n_{Tan}	2.0294	Tantala refraction index
E_{Tan}	140 GPa	Tantala Young modulus	ρ_{Tan}	$8015 \frac{kg}{m^3}$	Tantala density
ϕ_{Tan}	$1.9e - 4$	Tantala losses	σ_{Tan}	0.23	Tantala Poisson ratio
$\phi_{SilCoat}$	$2e - 5$	Coated silica losses	Temp	300 K	Temperature

Table 3: Table of parameters used for the thermal noise estimation. Mirrors have been assumed half infinite. Thermoelastic and thermorefractive effects on coatings have not been considered here. Ribbon losses have been kindly given by A. Heptonstall from Glasgow.

12.3 Ears machining

Machining the ears out of the lateral surface of the test mass is not a new idea but it was almost immediately discarded for two main reasons: i) in case one ear breaks a new mass has to be machined and coated; ii) complex machining causes an increase of surface losses on the test mass.

The project proposed here is an attempt to find a solution to the problems mentioned above. Although it is not possible to avoid the ear breaking, yet it is possible to shape the ear in a particular way in order to cause the breaking in a selected point. For instance, if the ear has the shape of a cone it will be almost impossible to have an accidental break close to the base of the cone. With a more refined shape it could be possible to have the break on a part of the ear that has a suitably small cross section. In this case it is not hard to imagine to melt fused silica on top of the broken ear until a new welding point is constituted again. The shape of the new ear is not relevant for the thermal noise performance and the positioning error on the welding points in general are comfortably large.

The proposed R&D work aims to demonstrate that it is possible to suitably shape the ear and to add fused silica once the ear is broken. Moreover it should be found a geometry easy to machine and demonstrate that the surface quality is sufficiently good for thermal noise performance.

12.3.1 Status of the related R&D

An R&D activity has already been performed in the Virgo+ frame for the suspension of the 20 kg mirrors. For a detailed description of this activity refer to the Virgo+ Review document. A new part related to the use of heavier mirrors and ribbon suspension has still to be started within the Virgo project. There is an open activity of the Glasgow group financed by EGO on the ribbon option.

12.4 Mirror local control system

An upgraded mirror local control system has to be implemented in order to take into account the new monolithic last stage suspension, actuation systems and interferometer configuration. To this aim the study and design must be performed with the new specifications for the Locking and Automatic Alignment purposes.

12.4.1 Status of the R&D

An activity aimed to study the modification due to the presence of the monolithic suspensions is already being carried on in the frame of the Virgo+ project. A detailed description can be found on the Virgo+ review document.

Advanced Virgo Conceptual Design:

PART 3:

Electronics, Vacuum, Facilities

13 Electronics, controls and data acquisition

An important R&D work has already been done within the Virgo collaboration to fulfill the requirements of controls and change obsolete systems for the Virgo+ project. This program was mainly focused on increasing the computing power available for sensing, alignment, and suspensions controls. The main modifications for the Virgo+ are :

- increasing of the computing power for suspensions using 6 more powerful DSPs instead of one (current situation);
- increasing of the computing power for photodiodes readout and global control systems by using real time Linux PC instead of the present RIO architecture associated with LynxOS;
- changing the connection with optical links to increase data flux and the timing system to ensure time tagging for all ITF subsystems;
- changing ADCs for sensing to gain one order of magnitude for dynamics;
- changing DACs and coil drivers to decrease noise actuation.

These modifications will allow an increase of the control loop frequency, if it is requested for sensing and alignment and could allow the use of more aggressive filters with better margins.

These systems have been designed to be used also for AdV and are easily upgradable with more powerful CPU when they will be available; a possible change of DSPs could be also foreseen taking into account at least one year time for development and tests.

The electronics deployment plan for Virgo+ has already taken into account the signal recycling mirror in the optical configuration.

Despite the R&D already covered, some technical limitations could still have an impact on the sensitivity of AdV mainly with actuation noise related to DAC chips already available. Future DAC may deliver chips with more bits and an higher frequency, which will be useful to achieve the design sensitivity in the low frequency band.

Length sensing and controls will be done using synchronous modulation/demodulation technique (RF) but gravitational-wave output will use a DC detection technique (see sec. 8). In case of signal recycling configuration the use of an RF technique on the dark port could be done. The noise introduced by the demodulation boards will not be limiting Virgo sensitivity if we use the same demodulation frequency, while higher frequencies can introduce more noise and must be studied. Possible developments can be considered for replacing such analog system by digital ones and provide more flexibility. Virgo has already experienced the use of an output mode-cleaner, needed for the DC detection, which may require some upgrades of its control given the higher finesse.

To improve controls for AdV, a new strategy could be implemented offering provisions for data exchange between alignment and length control systems. It could be already available for Virgo+. New ways of designing filters and controls for the interferometer

can also be tested and implemented to help in the commissioning phase of the instrument. At least using the same framework for the online software development will allow to avoid waste of manpower. New solutions will be tested and checked to verify if they fulfill the present performances.

In Virgo we still use some analog loops to control the laser (first and second stage of frequency stabilization) and in part of the mode cleaner. These subsystems could migrate to digital solutions for AdV. This choice could simplify the upgrade and modification of the filters applied to these loops.

Others subsystems will need to be changed as they will become obsolete and/or too difficult to maintain. In this category we found the CCD camera used for local controls, beam monitoring, and output mode cleaner lock, the vacuum control system which is based on OS9 machines no more maintained today. These changes will need new R&D programs that should start as soon as possible. A change of the power supplies will be planned to try to reduce as much as possible our coupling with environmental noises, a new power distribution architecture could be implemented.

Virgo evolution will benefit from the adoption of official standards in designing electronics, standards that will allow to manage effectively the various phases from conceptual design to installation one, including maintenance. These standards will address of course the safety of custom designed electronic equipment first and then the functional (electrical, mechanical) and operational interfaces among subsystems. Peculiar attention will then be devoted to the so far overlooked issue of Electro-Magnetic Compatibility, both applying the appropriate guidelines to the new designs, from their schematic development on, and evaluating suitable measures for mitigating shortcomings of the existing ones, at the board and system levels, wherever present.

The system of data acquisition will be upgraded by changing the machines used today in order to deal with a data flux increase by a factor 2 to 4 compared to the present situation. Possible problems could come from available space for storage part and from access to the disks. The network available will not be a limiting factor as 2 Gb connection are available between the Central building and the Control building, only the 100 Mb network inside the Central building could be easily upgraded to a 1 Gb one.

Other improvements for AdV could be decreasing the latency for accessing the data and developing new tools for visualization. As signals up to tens of MHz are used in Virgo control scheme, it will be useful to have the possibility to visualize some signals up to these frequencies to help debugging problems.

One of the main concerns for DAQ in AdV will be the increase in flux of data needed to be transferred from site to computing centers. This will require the increase of the outside network bandwidth and may be the use of better compression algorithms to optimize the size of files, and also the use of processed data, to reduce the number of channels stored in the files.

14 Vacuum system modifications

14.1 Requirements

In AdV the waist of the gaussian beams will be set in the center of the cavities; the average radius of the beam impinging on the central and terminal mirrors is assumed to be 60 mm. The rule of thumb for minimum free apertures asks for a diameter of $2 \times 60 \times 2.5 = 300$ mm. This requires larger diameter link tubes (four) between the central towers, larger Brewster links (Input/PR and SR/Detection) and larger baffles in central and terminal towers (existing baffles have 230 mm apertures). The mentioned rule is valid for suspended optics, while a larger free aperture is required if optics are not seismically isolated. The correct aperture is to be determined. The lowest point of the AdV sensitivity curve: $3 \cdot 10^{-24} \sqrt{\text{Hz}}$ at 500-1000 Hz, corresponds to the residual gas noise at a pressure of $1.8 \cdot 10^{-6}$ mbar in the 3 km arm tubes, in case of H_2 only (see paragraph 30.2 in [57]); in case of a not baked system, the residual gas is essentially water vapor, requiring a lower pressure by a factor of about 2, due to the higher polarizability of the molecules. The presently attained base pressure of about $2 \cdot 10^{-7}$ mbar, in the unbaked tubes, corresponds to a safety factor of the order of 5 in residual gas pressure and of 2.5 in sensitivity. An additional pressure safety factor of 2-4 could be gained putting in operation all the pumps along the tubes or even doubling their number. Larger safety factors can be attained baking the system.

14.2 New link tubes

The most natural solution is to replace the existing link tubes (400 mm inner diameter with 250 mm valves and 230 mm glass baffles), with analogous ones but 600 mm in diameter, including the expansion bellows. The 250 mm valves shall be substituted with 500 mm valves and the 230 mm glass baffles (central and terminal towers) with larger ones. Also the 1 m tower flanges with a 250 mm or 400mm port have to be replaced with flanges respectively with 500 mm or 600 mm ports (two flanges per link). The selection of the size 600mm for the link tubes appears as a good choice between economic costs, easiness of installation, optical performances with respect to absorbing glass baffles number and positioning. The preferred size for the vacuum valve is 500 mm, instead of 600 mm, because this last one would involve a much more complex mechanical setup due to its dimensions, while not improving significantly the optical performances. The free aperture will be limited by the baffles to less than 500 mm (TBC).

The inspection in the Central Building confirmed that dismantling old links+flanges and installing new links+flanges requires to remove the two central panels and one lateral panel of the concerned oven walls. The new valves shall be installed inside the ovens in the same place of the old smaller valves, at the link end opposite to the expansion bellows. This operation will require between every tower pair:

- the installation of a plastic tent to preserve cleanliness;

- temporary disconnection/displacement of Ti pumps and measuring gauges and re-arrangement of cables;
- the installation of a service rail (bridge crane) to slide-in/slide-out tubes, valves and flanges.

This operation can be performed building all new links in advance and replacing the old ones one by one to reduce the possible pollution of towers. This operation will require a minimum of two working weeks per link, including vacuum test. The new links should be fired at 400 °C in order to reduce hydrogen outgassing rate, as it has been done for the whole UHV vacuum system. The link replacement has to be followed by vacuum tests and glass baffles installation. Only after these operations the new mirrors could be installed. Finally it has to be checked the present equipment blocking the towers to the building floor, being increased the vacuum forces acting on towers.

14.2.1 Baffles

In order to cover completely the link tube walls as seen by the beam spot on each mirror we need, instead of the existing three 230 mm glass baffles per link, about 4-5 baffles. The exact figure will be known once defined the needed aperture. Also the glass baffles in the towers, at each end of each link, need an aperture larger than the existing one, of 230 mm. The availability of the glass plate is being checked.

14.2.2 Brewster links

Two solutions are being studied:

- classical Virgo solution, with silica Brewster plate with a 300 mm aperture (the existing apertures are 196 mm at detection and 110 mm at injection); in this case no valves are needed
- cryogenic links to trap molecules migrating from the bench towers to the interferometer, without material on the beam path; in this case at least one valve per link is necessary.

14.3 SR tower

To support the SR mirror, it is necessary a long SA (see sec. 11.3); hence the tower has to *grow* by 3 vertical rings (viroles), while the *technical ring* is already there. Also the separating roof has to be built together with all its accessories.

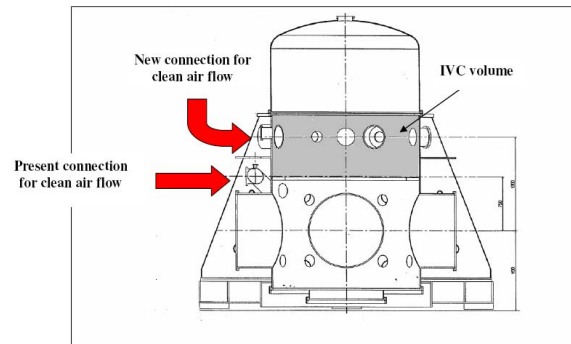


Figure 38: Technical drawing of the VIRGO base tower. The shaded area represents the IVC volume where the two plates are accommodated. The new connection for the clean air flow coming out from an absolute filtering system should be linked on the vacuum port available in between the IVC plates. In the picture the present clean air flow connection is indicated too.

14.4 UHV chamber improvements for AdV

The contamination reduction during the payload integration phase within the Ultra High Vacuum chamber is a crucial item. The surface mirror pollution, indeed, is responsible of the light absorption. Moreover, the non-perfect cleanliness conditions of the mirror create additional difficulties in the interferometer locking procedure and, as AdV is based on larger light power stored in the optical cavities, the interferometer may become uncontrollable.

During the integration phase, the long tuning procedure of the suspension system could be avoided introducing the Marionette Reference Mass installed within the UHV chamber. This element is tunable on bench minimizing the human intervention when it is hung to the filters chain (see sec. 11.5). In addition a better system to direct a quasi-laminar air flow within the vacuum chamber will have a positive impact on the mirror contamination. Profiting of the fact that on the two plates of the Intermediate Vacuum Chamber (IVC) four holes are available due to the Filter 7 legs removal, they could be used as aperture for a filtering system to be installed on the UHV chamber roof. Closing the holes on the top plate (tower upper part) by means of blind flanges, the second plate could support the vacuum shutters to be opened during the payload integration within the tower bottom part. The present cleaned air apparatus should be used to flow the clean air between the two plates (see fig. 38) forming the intermediate vacuum chamber toward the assembling payload. In this way the vacuum characteristic of the VIRGO tower is maintained. In fact, this intermediate vacuum chamber is necessary to allow a 2 orders of magnitude difference between the pressure of the upper and lower tower compartment. The tower vacuum volume operates with a differential pumping system while, during the payload assembly, a laminar air flow will be available within the UHV chamber. Other less invasive solutions are also being studied.

15 Infrastructure modifications for environmental noise reduction

The operation of Virgo has shown that some machine-induced noises leak out to the dark fringe signal. A noise hunting activity, aimed to understand the coupling mechanisms and find solutions, is in progress. However, in the perspective of having a detector 10 times more sensitive than Virgo, it would be safe to attenuate as much as possible the sources of noise. More silent machines can be installed to replace the existing ones. Further investigation is needed to understand whether some of them need to be moved far away from the experimental halls (Central building, West End Building, North End Building, Mode Cleaner Building). The machines that can be moved are:

- the air conditioning machines
- the water pumps
- the electric power generators
- the heat generators
- the air compressors
- the electric transformers
- the chillers
- the UPS machines

This would require new infrastructural works.

Acknowledgements

The Virgo Collaboration acknowledges that relevant contributions to this document have come from A.Freise and S.Hild of University of Birmingham, members of the GEO600 Collaboration. We look forward to continuing the fruitful collaboration with them.

References

- [1] R.Flamini, A.Freise, A.Gennai, P.Hello, P.La Penna, G.Losurdo, H.Lueck, N.Man, A.Masserot, B.Mours, M.Punturo, A.Spallucci, A.Viceré, *Advanced Virgo White Paper*, Virgo Internal report VIR-NOT-DIR-1390-304 (2005). 1
- [2] Advanced LIGO team, *Advanced LIGO Reference Design*, LIGO-M060056-06-M (2006). 1
- [3] <http://emvogil-3.mit.edu/bench/> 5
- [4] A.Buonanno, Y.Chen, gr-qc/0102012 (2001). 5
- [5] G.Losurdo, VIR-024A-07. 5, 39
- [6] G.M.Harry, *et al.*, *Class. Quantum Grav.*, **24** (2), 405 (2007) 5, 29
- [7] M.Beccaria, *et al.*, *Class. Quantum Grav.*, **15**, 3339 (1998). 5
- [8] J.D. Mansell *et al.*, *Appl.Opt.*, 40, 366-374 (2001) 16
- [9] LIGO T-060267-00-D (2006). 16
- [10] LIGO G-07011700-00-R (2007). 16
- [11] G.Mueller, LIGO T020021-00-D (2002). 16
- [12] P.Fritschel, LIGO T010075-00-D (2001). 16
- [13] *Input Optics Subsystem Preliminary Design Document*, LIGO-T060269-01-D 16
- [14] E. Khazanov *et al.*, *IEEE Journ. Quant. Electr.*, **35** (8), (1999) 18
- [15] E. Khazanov *et al.*, *Journ.Quant.Electr.*, **40** (10), (2004) 18
- [16] D.Tanner *et al.*, *The LIGO input optics*, LIGO-G070296-00-R 18
- [17] F.Acernese, *et al.* (The Virgo Collaboration), *Class. Quantum Grav.*, **21**, S395-S402 (2004). 21
- [18] N.Man, talk at the *Advanced Virgo workshop*, June 14th, 2007. 21
- [19] S.Hebri, Virgo Note VIR-NOT-EGO-1390-331 (2006). 22
- [20] The VIRGO Collaboration, *The Virgo Physics Book*, vol. II, Chap. 6 (2006). 22
- [21] S.Avino *et al.*, *Class. Quant. Grav.*, **23**, 5919-5925 (2006) 24

- [22] S. Avino et al, *Phys. Lett. A*, **355**, 258-261 (2006) [24](#)
- [23] http://www.virgo.optique.espci.fr/Virgo_Mirrors/ [28](#)
- [24] A.Brillet, *et al.*, *Phys. Rev. D*, **67**(10), 102006 (2003) [28](#)
- [25] A.Rocchi, talk at the LSC-Virgo Meeting, Cascina May 24, 2007. [34](#)
- [26] P.Willems, LIGO-T060224-00D (2006). [34](#), [35](#)
- [27] M.Smith, P.Willems, Auxiliary Optics Support System Conceptual Design Document, Vol. 1 Thermal Compensation System, LIGO-T060083-01-D [35](#)
- [28] T.L.Kelly, *et al.*, *Appl. Opt.*, **46**(6), 861-866 (2007) [36](#)
- [29] J.Y.Vinet, talk at the Advanced Virgo Workshop, Cascina June 14, 2007. [36](#)
- [30] E. Tournefier, *Technical noises for Virgo+: DC and AC readout cases*, VIR-NOT-LAP-1390-338 [38](#), [40](#)
- [31] A. Buonanno, Y. Chen, *Phys.Rev. D* **64**, 042006 (2001) [42](#)
- [32] D.E. McClelland et al., *Phys Rev D***48**, 5475 (1993) [43](#)
- [33] R. N.Mavaddat et al., *J. Optics (Paris)* **26**, 145 (1995) [43](#)
- [34] E. D'Ambrosio, R. O'Shaughnessy, S. Strigin, K.S. Thorne and S. Vyatchani, gr-qc/0409075 (Sept. 2004) [44](#)
- [35] Y. Pan gr-qc/0608128 (Aug. 2006) [44](#)
- [36] G. Müller and S. Wise, LIGO document Number T020026-00-D, <http://www.ligo.caltech.edu/docs/T/T020026-00.pdf> [44](#)
- [37] J. Mizuno, Ph.D. thesis Max Planck Institute für Quantenoptik, Garching 1995 [45](#)
- [38] A.E.Siegmann, *Lasers*, Oxford Univ. Press (1989) [47](#)
- [39] Y.Levin, *Phys. Rev. D*, **57**, 659 (1998) [47](#)
- [40] F.Bondu, *et al.*, *Phys. Lett. A*, **246**, 227 (1998) [48](#), [51](#)
- [41] J.Y.Vinet, *Class. Quant. Grav.*, **24**, 3897 (2007) [50](#)
- [42] E.D'Ambrosio, *Phys. Rev. D*, **67**, 102004 (2003) [50](#)
- [43] J.Y.Vinet, to be published in *Living reviews* [50](#), [51](#), [52](#)
- [44] B.Mours, *et al.*, *Class. Quant. Grav.*, **?**, 5777 (2006) [51](#)
- [45] V.Braginskij, *et al.*, *Phys. Lett. A*, **264**, 1 (1999) [52](#)
- [46] CALVA Conceptual Design, https://edms.in2p3.fr/file/I-010870/2/Conceptual_Design.pdf [56](#)
- [47] G. Losurdo, D. Passuello, P. Ruggi, VIR-NOT-FIR-1390-318 (2006). [62](#)
- [48] P.Puppo and P.Rapagnani, VIR-NOT-ROM-1390-311 [67](#)

- [49] P. S. Linsay, D. H. Shoemaker, *Rev. Scient. Instrum.* **53** (1982) 1014. 68
- [50] H. Luck *et al.*, *Status of the GEO600 detector*, *Class. Quant. Grav.* **23** (2006) S71. 68
- [51] S. Grasso, C. Altucci, F. Barone, V. Ragozzino, S. Solimeno, T. Pham, J. Y. Vinet, R. Abbate, *Phys. Lett. A* **244** (1998) 360. 68, 69, 70
- [52] P. Amico, L. Bosi, L. Carbone, L. Gammaitoni, M. Punturo, F. Travasso, and H. Vocca, *Class. Quant. Grav.* **19** (2002) 1663-1668. 68
- [53] V. P. Mitrofanov, N. A. Styazhkina and K. V. Tokmakov, *Class. Quant. Grav.* **19** (2002) 2039-2043. 68
- [54] S. Rowan, S. Twyford, R. Hutchins and J. Hough., *Class. Quant. Grav.* **14** (1997) 1537-1541. 68
- [55] M. J. Mortonson, C. C. Vassiliou, D. J. Ottaway, D. H. Shoemaker, and G. M. Harry, *Rev. Scient. Instrum.* **74** (2003) 4840-4845. 68
- [56] V. P. Mitrofanov, L. G. Prokhorov and K. V. Tokmakov, *Phys. Lett. A* **300** (2002) 370. 69
- [57] Virgo Collaboration, *Virgo Final Design* (1997). 83